ERDC/GSL TR-15-28

US Army Corps
of Engineers®
Engineer Research and
Development Center

ERDC
INNOVATIVE SOLUTIONS
for a safer, better world

Airfield Damage Repair Modernization Program

AM2 Mat End Connector Modeling and Performance Validation

Lyan Garcia, Timothy W. Rushing, Quint Mason, Jeb S. Tingle,
and Craig A. Rutland

August 2015

Geotechnical and Structures Laboratory

The U.S. Army Engineer Research and Development Center (ERDC) solves the nation's toughest engineering and environmental challenges. ERDC develops innovative solutions in civil and military engineering, geospatial sciences, water resources, and environmental sciences for the Army, the Department of Defense, civilian agencies, and our nation's public good. Find out more at www.erdc.usace.army.mil.

To search for other technical reports published by ERDC, visit the ERDC online library at http://acwc.sdp.sirsi.net/client/default.

ERDC/GSL TR-15-28
August 2015

AM2 Mat End Connector Modeling and Performance Validation

Lyan Garcia, Timothy W. Rushing, Quint Mason, and Jeb S. Tingle

Geotechnical and Structures Laboratory
U.S. Army Engineer Research and Development Center
3909 Halls Ferry Road
Vicksburg, MS 39180-6199

Craig A. Rutland, Ph.D.

Engineering Division
Civil Engineering Branch
Air Force Civil Engineering Center
139 Barnes Drive, Suite 1
Tyndall AFB, FL 32403

Final report

Prepared for Headquarters, Air Force Civil Engineer Center
Tyndall Air Force Base, FL 32403-5319

Abstract

The U.S. Army Engineer Research and Development Center executed a test program for the Air Force Civil Engineer Center and the Naval Air Systems Command that involved a series of full-scale tests of the AM2 airfield mat system in an effort to validate a model that can predict the performance of AM2 under different operational conditions. After completion of the program, a thorough investigation of both the subgrade and the mat revealed that the manufacturer's drawing of the extrusion die for the AM2 end connector omitted fillets in the corners of the locking bar channel. The efforts of the test program discussed in this report focused on evaluating AM2 with the two different end connector designs (i.e., filleted and non-filleted locking bar slot) and evaluating the performance of each in terms of number of passes to failure. Two sections were tested individually under simulated F-15E aircraft traffic. Mat breakage and permanent deformation were monitored. The AM2 end connector design with the filleted corners was able to sustain more than twice the traffic sustained by the non-filleted design before failure by both permanent deformation and mat breakage.

Contents

Figures and Tables

Figures

Tables

Preface

This study was conducted for the U.S. Air Force Civil Engineer Center (AFCEC) and the U.S. Naval Air Systems Command (NAVAIR) Expeditionary Airfield (EAF) team. Technical oversight was provided by Jeb S. Tingle.

The work was performed by the Airfields and Pavements Branch (APB) of the Engineering Systems and Materials Division (ESMD), U.S. Army Engineer Research and Development Center, Geotechnical and Structures Laboratory (ERDC-GSL). At the time of publication, Dr. John F. Rushing was Acting Chief, APB; Dr. Larry N. Lynch was Chief, ESMD; and Nicholas Boone was the Technical Director for Force Projection and Maneuver Support. The Acting Deputy Director of ERDC-GSL was Dr. Gordon W. McMahon, and the Acting Director was Dr. William P. Grogan.

LTC John T. Tucker III was the Acting Commander of ERDC, and Dr. Jeffery P. Holland was the Director.

Unit Conversion Factors

Multiply	By	To Obtain
cubic feet	0.02831685	cubic meters
feet	0.3048	meters
inches	0.0254	meters
kip-inches	112.948	newton-meters
pounds (force)	4.448222	Newtons
pounds (force) per square foot	47.88026	pascals
pounds (force) per square inch	6.894757	kilopascals
pounds (mass)	0.45359237	kilograms
square feet	0.09290304	square meters
square inches	6.4516 E-04	square meters

1 Introduction

1.1 Background

AM2 aluminum matting has been the primary airfield matting system used by the U.S. military since the late 1960s. AM2 was developed by the U.S. Navy, but has been adopted for use by the U.S. Air Force (USAF) and U.S. Army for fixed-wing and rotary-wing operational surfaces. Over the years, AM2 has been modified to address limiting structural concerns. The current production version of AM2 is modification (Mod) 5.

An AM2 surface is comprised of interlocking 2-ft by 12-ft full panels and 2-ft by 6-ft half panels that are 1.5 in. thick. AM2 mat can be assembled to form runways, vertical takeoff and landing pads, taxiways, and aircraft parking areas. In 2012, The Naval Air Systems Command (NAVAIR) Expeditionary Airfield (EAF) Team partnered with the Air Force Civil Engineer Center (AFCEC) to sponsor a series of full-scale AM2 evaluations in an effort to validate a Dynamic Interface Model (DIM) developed by NAVAIR. The model was initially validated through laboratory subscale tests, but additional development and validation was required to accurately model the matting subsurface and soil interaction for various installation patterns. The U.S. Army Engineer Research and Development Center (ERDC) was tasked with these evaluations. Individual AM2 configuration lay patterns (brick-work, 2-1, and 3-4) were tested under simulated traffic with appropriate instrumentation at the connections to collect strain data for the DIM. Descriptions of each pattern are provided in NAWCADLKE-MISC-48J200-0011 (2006). Each test was compared to baseline performance data from full-scale testing conducted at the ERDC Vicksburg, MS site from 2005 through 2011 (Table 1).

Table 1. Summary of AM2 brickwork pattern subgrade sensitivity testing results.

Sustained Traffic Passes			
Subgrade Strength (CBR)	F-15E	C-17	Reference
6	1,500	1,500	Rushing and Tingle (2007)
10	3,000	6,000	Rushing et al. (2008)
15	4,100	7,000	Rushing and Mason (2008)
25	6,300	10,000[a]	Garcia et al. (2014a)
100	23,000	---[b]	Garcia et al. (2014b)

[a] Failure was not achieved. Trafficking was stopped because of time constraints.

[b] Not tested.

After completion of the test program, a thorough investigation of both the subgrade and the mat revealed that the manufacturer's drawing used for the extrusion die for the AM2 end connector inadvertently omitted filleted corners in the locking bar channel. As shown in Figure 1, this location is the smallest cross-sectional area of the rail.

Several modeling efforts showed that these corners were areas of high stress concentration, shown in Figure 2. In Figure 2a, the load (i.e., F-15E tire load) is applied on the right side of the joint. In this case, the load is transferred to the lower overlap rail through the locking bar, and a high tensile stress is shown at the corner adjacent to each rail. In Figure 2b, the load is applied on the left side of the joint. In this case, the loading results in a compressive stress at the internal rail radii at the locking bar corners. In both cases, critical stresses developed at the locations shown in Figure 1, which is consistent with rail breakage commonly reported by Rushing and Tingle (2007), Rushing and Torres (2007), Rushing et al. (2008), Rushing and Mason (2008), and Garcia and Rushing (2013). An example of crack initiation at one of the corners is shown in Figure 3.

The die was recently corrected after an unknown period of producing the non-filleted design. Researchers questioned whether this fillet omission might have affected the performance of AM2 throughout the NAVAIR and AFCEC test program. Based on modeling results, it was assumed that a filleted corner would reduce stress concentrations at these locations and provide better fatigue life of the rails. Therefore, AFCEC sponsored the evaluation discussed in this report to quantify the difference in performance (if any) between AM2 produced without the filleted corners in the locking bar channel and a production lot with the filleted corners. NAVAIR provided mats representing AM2 panels without the filleted corners and ALFAB, Inc. provided panels produced with the filleted corners.

1.2 Objective and scope

A production version of AM2 panels with filleted corners in the locking bar slot was tested side by side with a section of AM2 having the non-filleted corners to compare their performance in terms of allowable passes to failure. The objective of the evaluation was to determine whether an appreciable difference could be observed in the performance of AM2 with the filleted design of the locking bar channel. A full-scale test section having a 36-in.-deep subgrade prepared to a California bearing ratio (CBR) of 6 was surfaced with AM2 matting of both designs and divided

into two test items that were both subjected to simulated F-15E traffic. The results of AM2 panels manufactured with non-filleted corners in the locking bar channel were compared to the results of AM2 panels produced with the correct design.

Figure 1. Corners (a) without fillet; (b) with fillet.

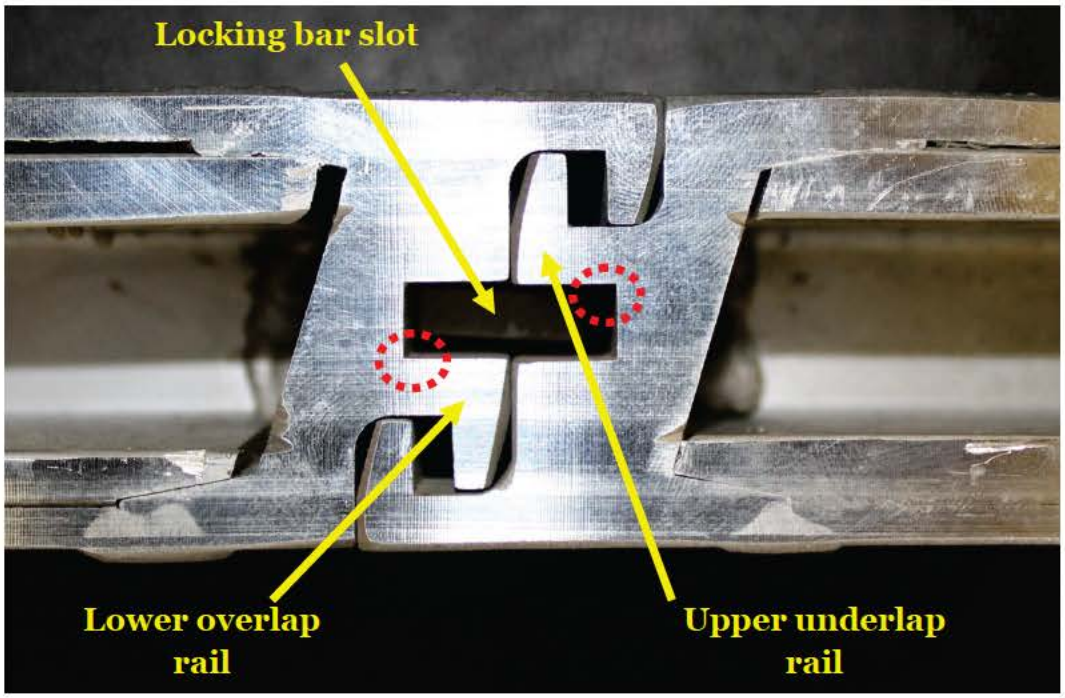

(a)

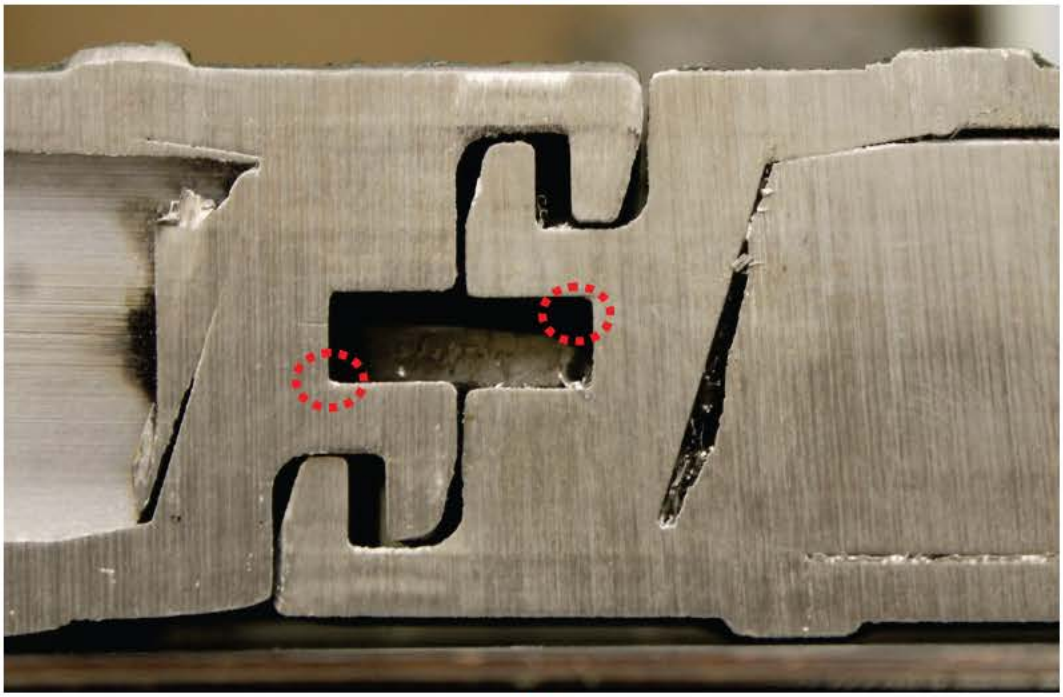

(b)

Figure 2. AM2 joint modeling analysis: (a) load on right side; (b) load on left side.

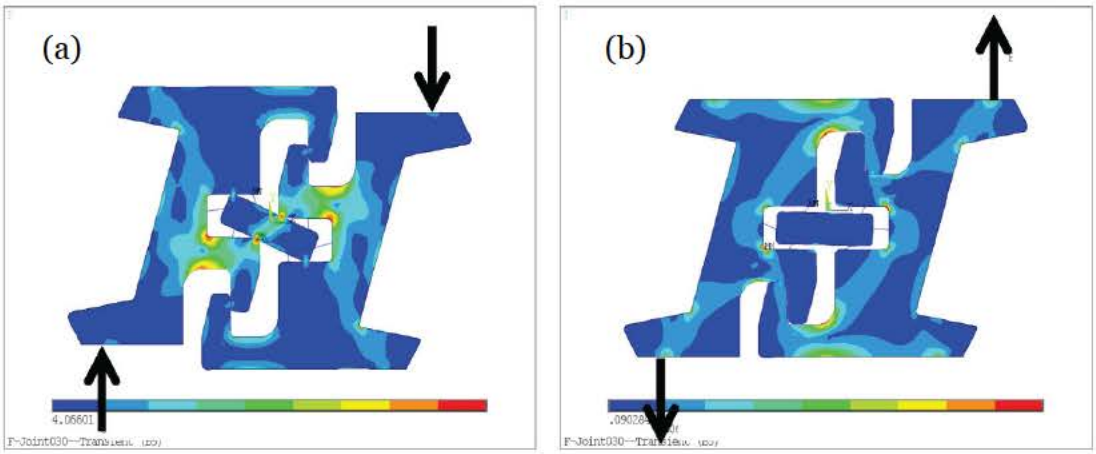

Figure 3. Crack initiation at lower overlap rail.

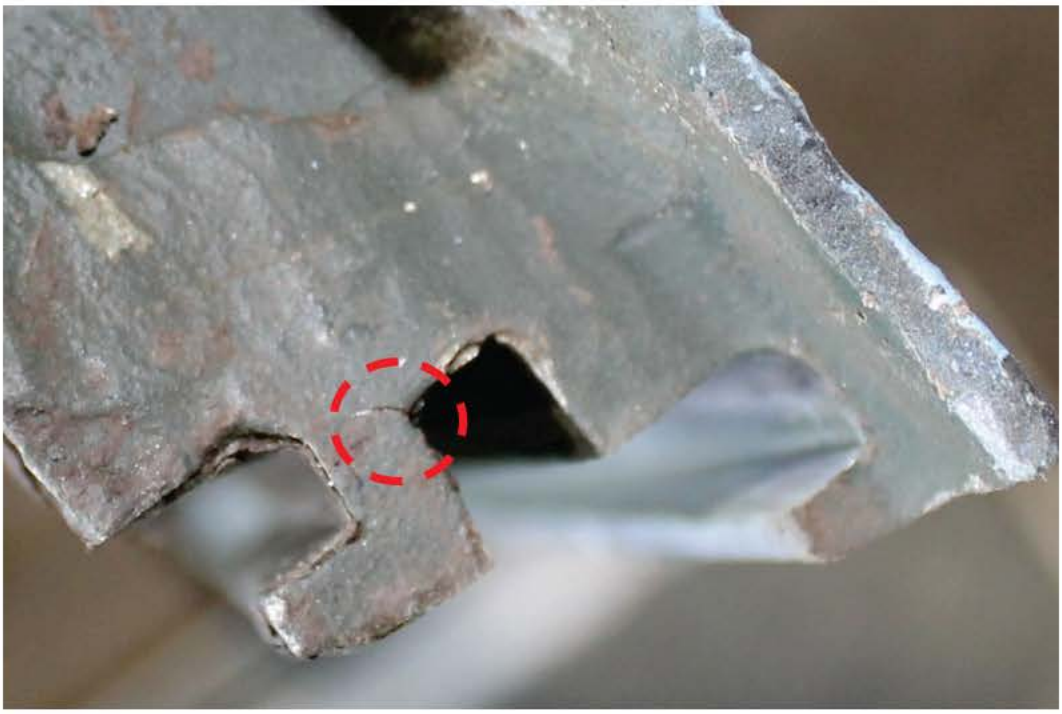

2 Materials

2.1 AM2 airfield mat

AM2 airfield mat was developed in the 1960s under a program sponsored by the Naval Air Engineering Center, in Philadelphia, PA. Various versions of AM2 were tested under simulated aircraft loads at the U.S. Army Engineer Waterways Experiment Station in Vicksburg, MS (known today as ERDC), from 1961 through 1971, with major procurements beginning in 1965. The original AM2 mat has been modified through the years to address limiting structural concerns. The current production version of AM2 is Mod 5.

AM2 panels are 2 ft by 12 ft by 1.5 in. and are fabricated from a single 6061-T6 aluminum alloy extrusion with end connectors welded to the 2-ft ends to form a complete panel. The core of the extruded panels is comprised of vertical stiffeners spaced 1.75 in. apart in the 12-ft direction. The mat is also made in half-panels to allow for placement of a staggered brickwork configuration. The panels were joined along the two 12-ft edges by a hinge-type male/female connection. The adjacent 2-ft ends were joined by an overlap/underlap connection secured by an aluminum locking bar. The panels were coated with an antiskid material to increase the surface friction. Pertinent properties of AM2 mat are shown in Table 2.

AM2 panels produced without the filleted corners were manufactured in October 2013 and were supplied by NAVAIR. The AM2 panels including the filleted corners were manufactured in 2014 and supplied by ALFAB, Inc. A panel supplied by ALFAB, Inc. was cut and inspected to verify that the end connector was restored to its correct design. The delivered panels are shown in Figure 4.

Table 2. AM2 mat properties.

	Full-panel	Half-panel
Length (ft)	12	6
Width (ft)	2	2
Thickness (in.)	1.5	1.5
Panel Weight (lbf)	145.5	74.4
Unit Weight (lbf/ft^2)	6.1	6.3

Figure 4. NAVAIR F71 package (left) and ALFAB, Inc. AM2 bundles (right).

2.2 High-plasticity clay (CH) subgrade

A high-plasticity clay (CH) material was used for subgrade construction and procured from a local source in Vicksburg, MS. The CH material was subjected to laboratory tests listed in Table 3. Classification data for the subgrade soil are shown in Figure 5. CBR-moisture and moisture-density content relationships are shown in Figures 6 and 7, respectively. These data were used to determine the target moisture content and dry density required to obtain the target CBR of 6.

Table 3. Laboratory tests for Vicksburg Buckshot CH.

Test Name	ASTM
Standard Practice for Classification of Soils for Engineering Purposes (USCS)	D 2487
Standard Test Method for Particle Size Analysis of Soils	D 422
Standard Test Method for Laboratory Compaction Characteristics of Soil Using Modified Effort	D 1557
Standard Test Method for CBR of Laboratory Compacted Soils	D 1883
Standard Test Methods for Liquid Limit, Plastic Limit, and Plasticity Index of Soils	D 4318

Figure 5. Gradation curve for Vicksburg Buckshot CH.

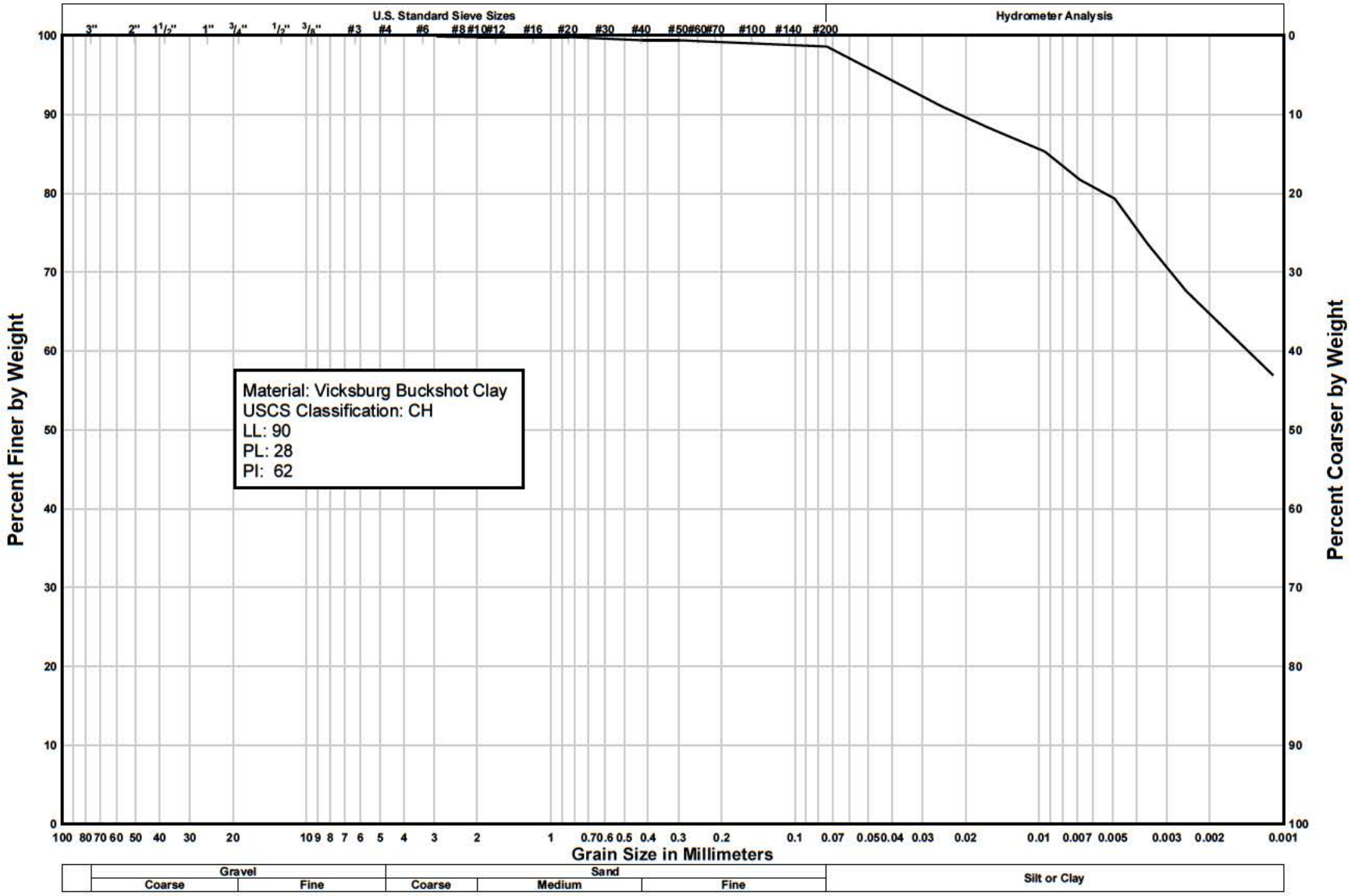

Figure 6. CBR vs. moisture content for CH subgrade material.

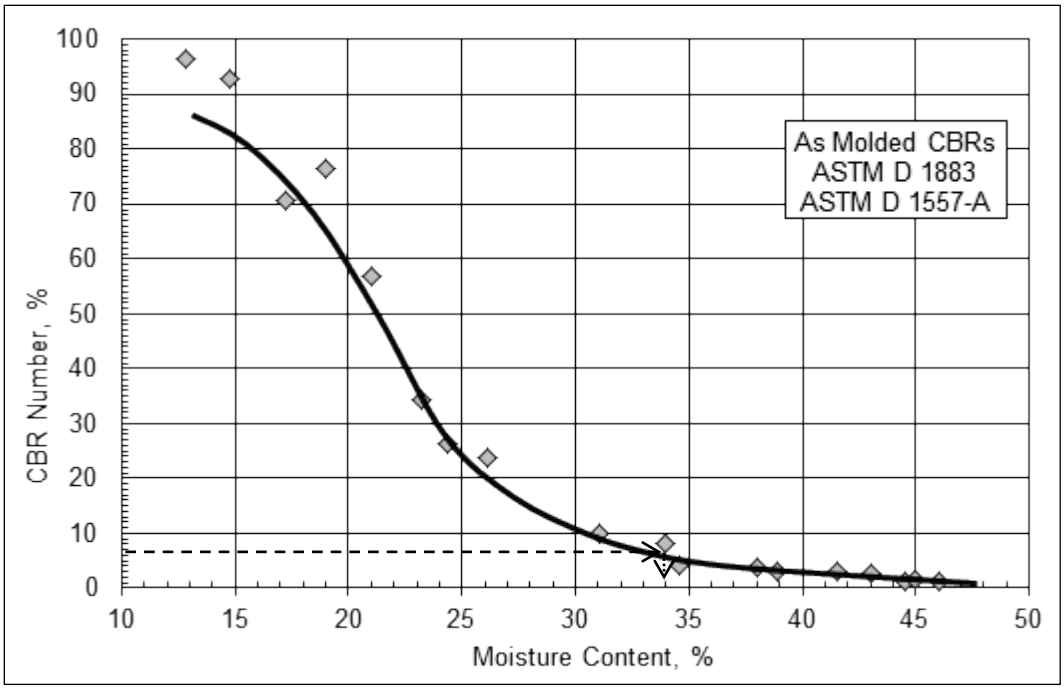

Figure 7. Dry density vs. moisture content for CH subgrade material.

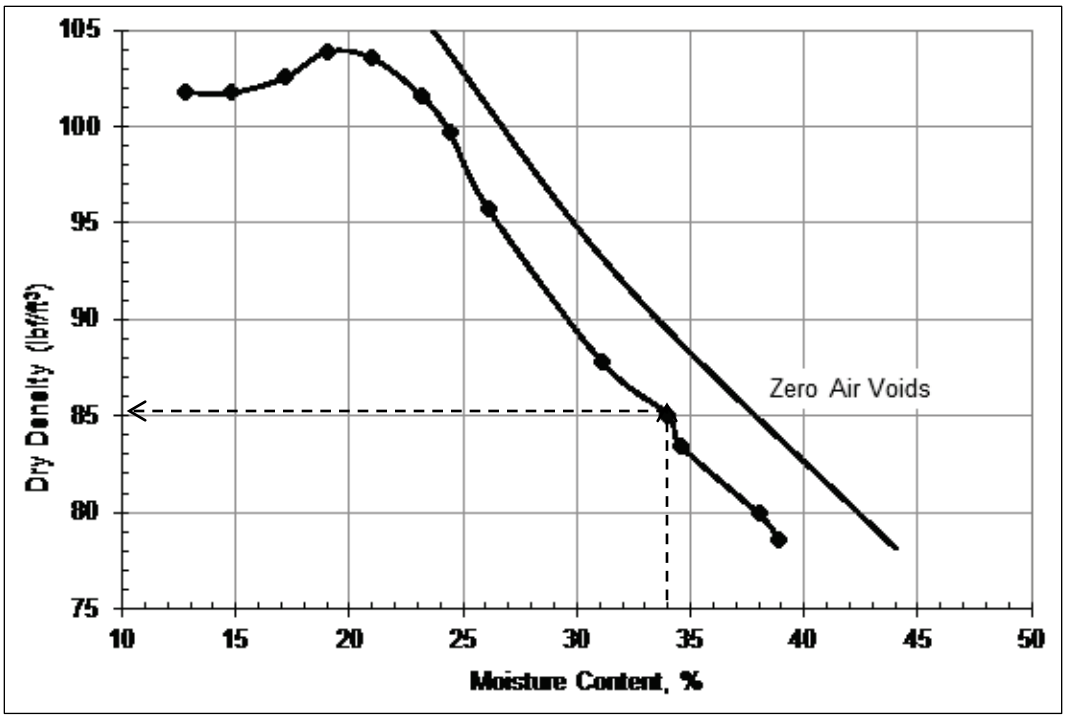

3 Experimental Program

3.1 Test section general description

A full-scale test section was constructed and trafficked under shelter in the Hangar 4 pavement test facility at ERDC. AM2 mat panels were placed directly over a 36-in.-deep CH subgrade prepared to a CBR of 6 over an existing silt foundation, as shown in Figure 8. A general layout of the test section along with panel designations is shown in Figure 9.

Each panel was identified with a number to track damage during trafficking. The matting surface was 48 ft wide by 42 ft long and was subsequently divided into two 24-ft-wide test items. The item on the west side of the test section consisted of the non-filleted version of AM2, designated Item A. The east test item consisted of panels manufactured with the filleted corners, designated Item B. Since a limited number of filleted AM2 panels were provided by ALFAB, Inc., panels that were not subjected to traffic in Item B were provided by NAVAIR (e.g., panel I3). Each test item had a 3.75-ft-wide lane designated for simulated F-15E traffic. Traffic was applied in a normally distributed wander pattern associated with the F-15E.

3.2 Test section construction

The following sections describe the construction of the foundation sub-grade and the AM2 mat installation. Field and laboratory soil testing data used to determine the moisture, density, and bearing capacity in terms of CBR are also included.

Figure 8. Test section profile.

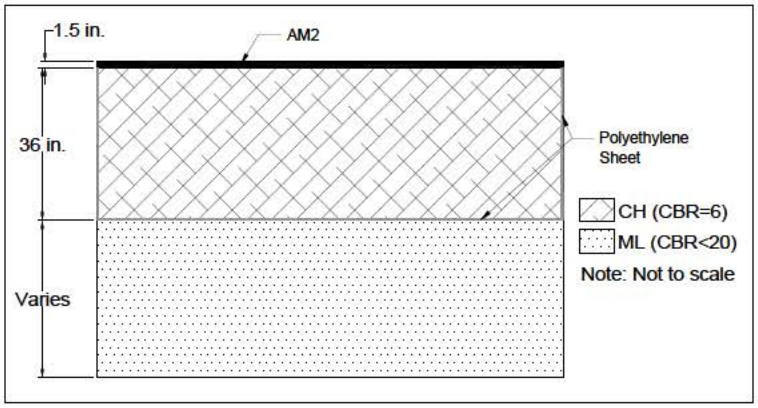

Figure 9. AM2 panel layout.

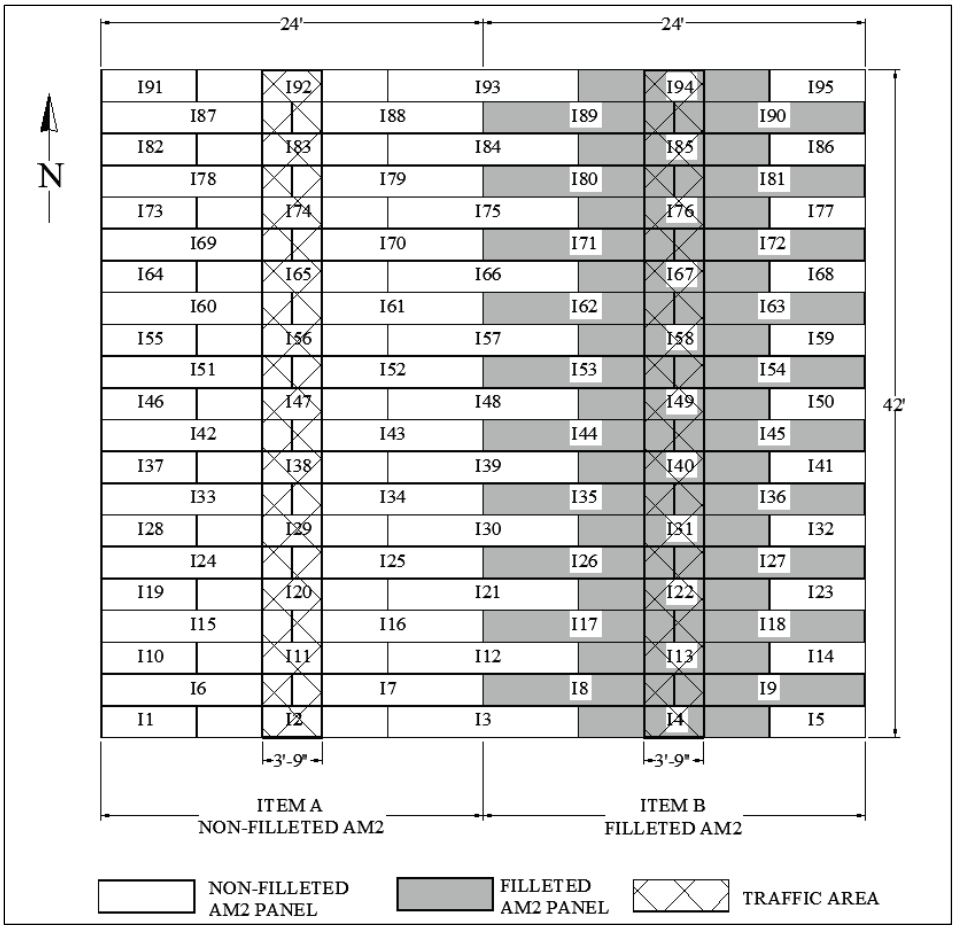

3.2.1 Subgrade construction and posttest forensics

The test section subgrade was built using in-place material from a previous AM2 test section constructed to a CBR of 6. The original subgrade was constructed by excavating a 60-ft-wide by 42-ft-long test pit to a minimum 36-in. depth below the existing finished grade in Hangar 4, as shown in Figure 10. The soil at the bottom of the excavation was a silt material (ML) having a CBR less than 20.

The existing ML material was leveled with a bulldozer and compacted with a pneumatic roller and a vibratory steel-wheel compactor to ensure that the remainder of the test section was constructed over a stable foundation. The bottom and sides of the test pit were lined with impervious 6-mil polyethylene sheeting to minimize moisture migration from the 36 in. of new CH soil serving as the test section subgrade, as shown in Figure 10.

Figure 10. Test section excavation (left) lined with impervious sheeting (right).

The CH was processed at a nearby preparatory site by spreading the material to a uniform 12-in. depth, pulverizing the material with a rotary mixer, adjusting the moisture content, pulverizing the material again, and stockpiling it, as shown in Figure 11. This was an iterative process necessary to achieve a uniform distribution of moisture throughout the material. Once the CH had been processed to the target moisture content, it was placed in the test section, spread by a bulldozer in 8-in. lifts, and compacted with a pneumatic roller to a thickness of 6 in., as shown in Figure 12. Each compacted lift was subjected to the test methods listed in Table 4 to verify that target values had been met (Figures 13 and 14).

Table 4. Field tests on each constructed lift.

Test Name	Test Designation	Pre-test	Post-test
Standard Test Method for Density of Soil in Place by the Drive Cylinder	ASTM D 2937	X	
Standard Test Method for In-Place Density and Water Content of Soil and Soil-Aggregate by Nuclear Methods (Shallow Depth)	ASTM D 6938	X	X
Standard Test Method for Density and Unit Weight of Soil in Place by the Sand Cone Method	ASTM D 1556	X	
Standard Test Method for Laboratory Determination of Water Content of Soil and Rock by Mass	ASTM D 2216	X	X
Standard Test Method for Use of the Dynamic Cone Penetrometer in Shallow Pavement Applications *	ASTM D 6951	X	X
Standard Test Method for Determining the California Bearing Ratio of Soils	CRD-C 654-95	X	X

*Conducted after last lift was compacted.

Figure 11. Pulverizing CH (left) and adding moisture (right).

Figure 12. Leveling (left) and compacting (right) CH.

Figure 13. Nuclear gage (left) and sand cone (right) test.

Figure 14. Field CBR test.

In situ CBR tests (CRD-C 654-95) were conducted at six locations on every 6-in. compacted lift to verify that the target CBR of 6 had been reasonably achieved. If the average pretest CBR of a lift differed from the target value by more than +1.0 or -0.5 CBR, the lift was removed and reprocessed. Each lift was surveyed to obtain an average thickness. After data collection, the surface was scarified an average depth of 1 in. with a rotary mixer prior to placement of the following lift to facilitate bonding at the interface.

For the test discussed in this report, the upper 6 to 8 in. (approximately one lift) of an area 50 ft wide by 42 ft long of the existing test bed was removed and replaced with newly processed material. Posttest values from the previous evaluation taken 6 in. below the surface of the subgrade showed that the material retained its moisture and a CBR of approximately 6. It was assumed that the remainder of the subgrade depth retained its pretest values. Therefore, reconstruction of the entire depth was unnecessary. The newly processed material was replaced in one 6-in. lift. Field CBR, laboratory oven moisture, nuclear gage, and dynamic cone penetrometer (DCP) tests were performed at stations 10, 20 and 30 along the centerline of each test item to ensure the target values were achieved. The remaining tests listed in Table 4 were conducted at offset locations.

Once trafficking was completed, posttest forensics were conducted at the same locations to determine the depth of subgrade that might have undergone gradual drying and possible densification under traffic. Some increase in CBR was expected because of thixotropic properties of clay

structures and gradual drying and densification during trafficking. Based on historic testing data, surface increases of less than 5 CBR and increases of less than 3 CBR at a depth of 6 in. are common and acceptable (Rushing and Tingle, 2007; Rushing and Torres, 2007; Rushing et al., 2011; Garcia et al., 2012; Rushing et al., 2012).

Subgrade properties prior to installing mat and after completing trafficking on each test item are shown in Table 5. Changes in CBR on the surface and 6 in. below the surface were within ± 1 CBR. Additional testing below 6 in. was not required since the changes were within acceptable limits.

Table 5. Average in situ properties of the subgrade.

	Drive Cylinder		Sand Cone		Nuclear Gage			CBR		
Test Depth	Moisture %	Dry Density (lbf/ft³)	Moisture %	Dry Density (lbf/ft³)	Wet Density (lbf/ft³)	Dry Density (lbf/ft³)	Moisture %	Moisture %	In Situ CBR	Δ CBR
ITEM A										
PRETEST										
Surface [a]	35.5	83.1	34.5	88.9	117.0	88.1	30.1	33.7	5.8	-
6 in.	35.5 [c]	82.5 [c]	35.5 [c]	88.3 [c]	116.1 [b]	87.4 [b]	32.9 [b]	35.3 [b]	5.9 [b]	-
12 in. [c]	35.5	86.4	34.9	90.3	116.1	89.1	30.3	34.5	5.5	-
18 in. [c]	32.4	86.0	31.9	95.9	115.2	88.3	30.5	32.1	6.2	-
24 in. [c]	33.3	85.8	33.7	91.8	116.8	90.3	29.4	33.5	5.9	-
30 in. [c]	33.7	84.7	33.7	89.7	115.4	88.4	30.5	33.2	6.2	-
POSTTEST										
Surface	-	-	-	-	117.1	89.5	30.9	35.5	5.8	0.0
6 in.	-	-	-	-	115.4	88.5	30.4	34.7	6.5	0.6
ITEM B										
PRETEST										
Surface [a]	35.5	83.1	34.5	88.9	116.7	88.6	31.6	34.4	5.8	-
6 in.	35.5 [c]	82.5 [c]	35.5 [c]	88.3 [c]	116.4 [b]	87.4 [b]	33.2 [b]	34.9 [b]	5.9 [b]	-
12 in. [c]	35.5	86.4	34.9	90.3	116.1	89.1	30.3	34.5	5.5	-
18 in. [c]	32.4	86.0	31.9	95.9	115.2	88.3	30.5	32.1	6.2	-
24 in. [c]	33.3	85.8	33.7	91.8	116.8	90.3	29.4	33.5	5.9	-
30 in. [c]	33.7	84.7	33.7	89.7	115.4	88.4	30.5	33.2	6.2	-
POSTTEST										
Surface	-	-	-	-	115.9	88.7	30.8	35.8	5.6	-0.2
6 in.	-	-	-	-	117.0	90.4	29.5	35.0	6.7	0.8

[a] New compacted lift

[b] Measured after removing top lift of previous mat evaluation

[c] Average pretest values of previous mat evaluation

3.2.2 AM2 mat installation

The AM2 airfield mat system was placed on the surface of the prepared test section subgrade by an experienced crew. The mat bundles were placed on the test section with a forklift, and the individual panels were carried by two men and placed into position.

The first mat panel was placed flat on the ground with the long dimension perpendicular to the direction of traffic and with the male hinge connector facing north. The second panel was positioned adjacent to the 2-ft end of the first, allowing the overlapping end connector of the second panel to drop into position over the underlapping end connector of the first panel. A rectangular slot was formed between the two end connector rails, and an aluminum locking bar was inserted into the slot, as shown in Figure 15. This locking bar prevented the ends of the mat panels from separating. This process was continued until the first row was installed.

For the second row, the female hinge connector was attached to the male hinge connector of panels from the first row, and the panel was pivoted into place, as shown in Figure 16. The next panel was installed by attaching the female hinge connector to the male hinge connector of panels in the first row and allowing the overlapping end connector rail to pivot over and connect to the underlapping end connector rail of the adjacent panel. An aluminum locking bar was inserted into the space provided to keep the panels from separating. This process was repeated until the entire mat test section was assembled in a brickwork configuration with half-panels on alternating ends of every other row. Towing tubes, mandrels, and end caps available at ERDC from older U.S. Air Force Airfield Damage Repair kits were installed on the east and west edges of the test section to minimize shifting of the rows during traffic. These accessories are shown in Figure 17.

Once assembly was complete, full-panels of AM2 were installed along the ends of the traffic lanes to facilitate the entrance and exit of the test vehicles. Male keylocks were attached to the female hinge connector of the panels in the first row to facilitate ramp installation, as shown in Figure 18. A photo of the assembled test items is shown in Figure 19. Once the mats had been installed, 1,000-lb steel weights were placed along the edges of the test section to anchor the mats and simulate the resistance to movement provided by a large expanse of matting.

Figure 15. Insertion of aluminum locking bar between adjacent panels.

Figure 16. Installation of AM2 panels on the test section subgrade.

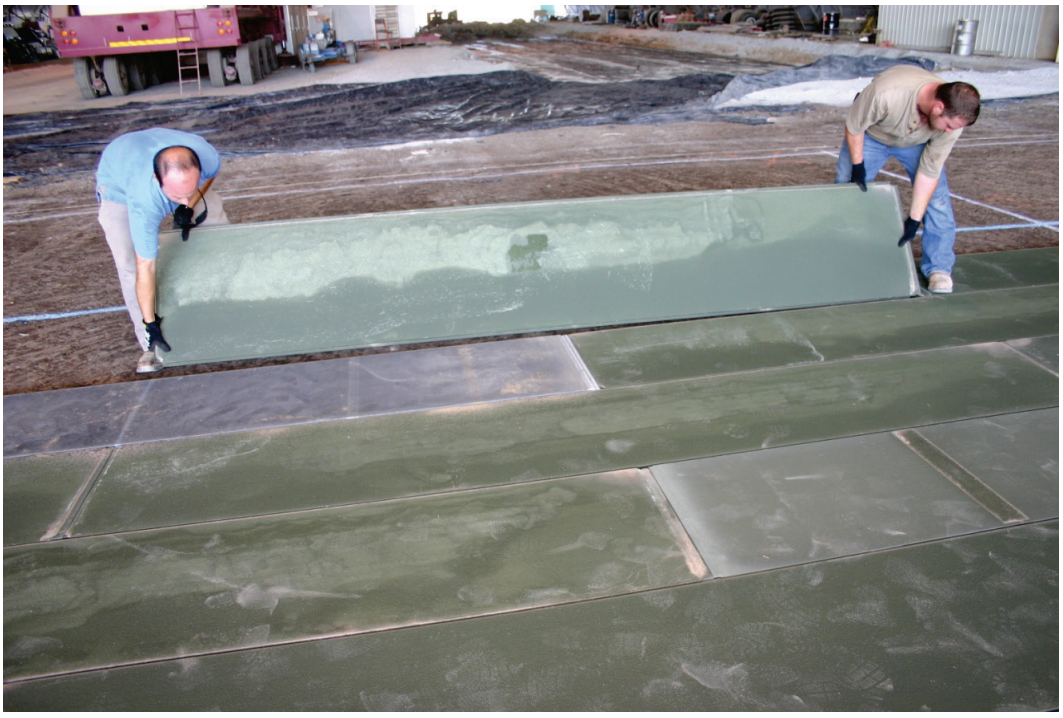

Figure 17. Typical installation of towing tubes to the edges of the test section.

Figure 18. Typical installation of male keylock.

Figure 19. Item A (left) and Item B (right).

3.3 Traffic application

A specially designed single-wheel load cart was used to simulate F-15E aircraft traffic. The load cart was equipped with a 36-in.-diam by 11-in.-wide, 30-ply tire inflated to 325 lbf/in.^{2} and loaded such that the test wheel was supporting 35,235 lb. The F-15E load cart was equipped with an outrigger wheel to prevent overturning and was powered by the front half of a U.S. Army 2.5-ton transport truck, as shown in Figure 20.

Figure 20. F-15E test load cart.

A normally distributed pattern of simulated traffic was applied in a 3.75-ft-wide traffic area for the F-15E test item, as shown in Figure 21. The traffic area was broken into five lanes that were designed to simulate the traffic distribution pattern, or wander width, of the main landing gear wheel on a mat surface when taxiing to and from an active runway. The width of each lane corresponded to the measured contact width, 9 in., of the F-15E tire when fully loaded and not the overall published tire width of 11 in. The normally distributed traffic patterns were simplified for ease-of-use by the load cart operator. Traffic was applied by driving the load cart forward and then backward over the length of the test item and then shifting the path of the load cart laterally approximately one tire width on each forward path. Tracking guides were attached to assist the driver in shifting the load cart the proper amount for each forward path. This procedure was continued until one pattern of traffic was completed. One pattern resulted in 16 passes, or 4 coverages.

Figure 21. Plan view showing F-15E normally distributed traffic lanes.

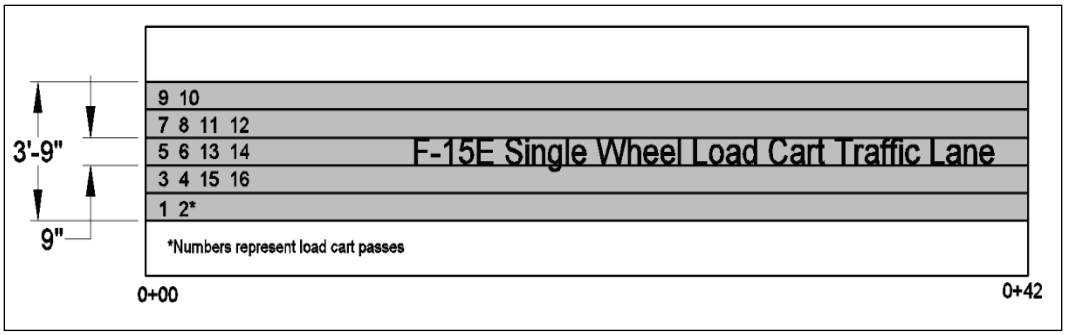

3.4 Data collection

Data collection in each test item included robotic total station measurements of the centerline profile, cross sections, and elastic deflection. Data were collected at the pass levels shown in Table 6. Data collection layouts are shown in Figure 22. The mat surface was inspected visually for damage periodically during trafficking.

Table 6. Data collection pass levels.

Total Passes	Profile	Unloaded Cross Sections	Loaded Cross Sections	Elastic Deflection
Pretest Subgrade	X	X		
0	X	X	X	
10	X	X	X	
16	X	X	X	X
32	X	X	X	X
48	X	X	X	X
112	X	X	X	X
240	X	X	X	X
496	X	X	X	X
1008	X	X	X	X
1232	X	X	X	X
1248	X	X	X	X
1520	X	X	X	X
2060	X	X	X	X
Posttest Subgrade	X	X		

Figure 22. Data collection layout.

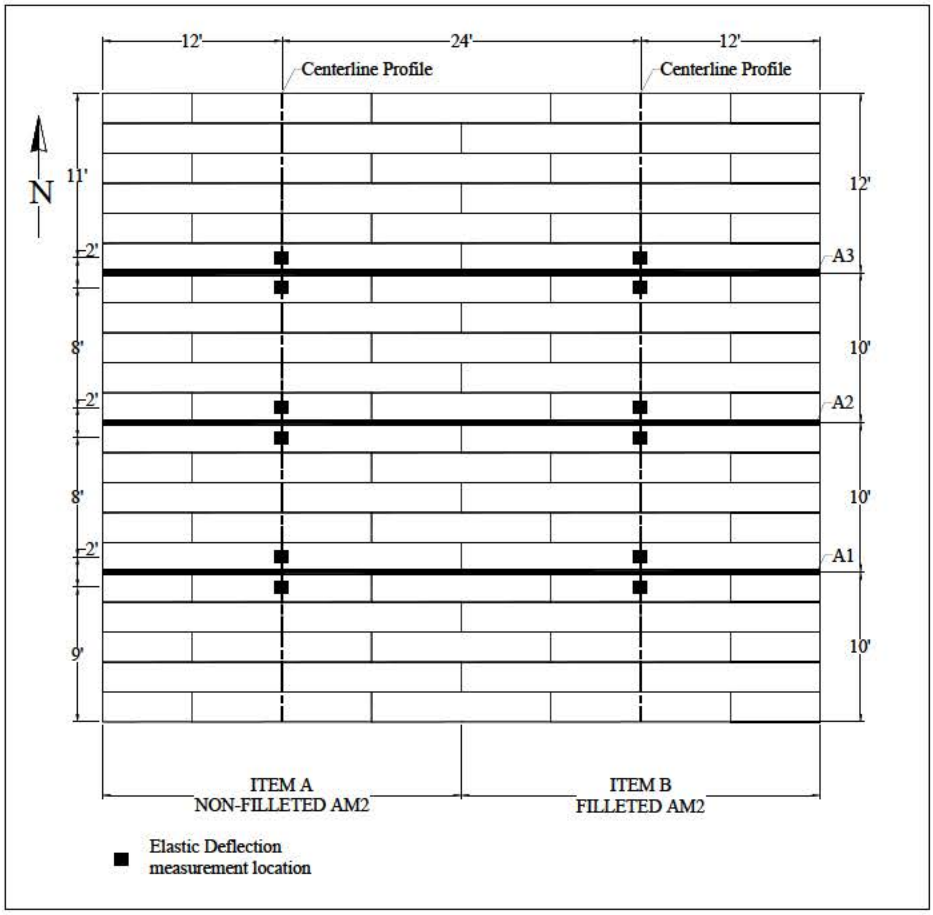

3.4.1 Centerline profile

Data collected along the traffic centerline are labeled "centerline profiles" in this report. These data were collected on the subgrade (Figure 23) prior to installing mat, on the mat surface prior to starting traffic and at scheduled pass levels during traffic, and on the subgrade surface after panels were picked up. Robotic total station elevation data were collected at 6-in. intervals on the subgrade and at 1-ft intervals on the mat surface.

3.4.2 Unloaded cross sections

Data collected transverse to the direction of traffic at the locations labeled A1, A2, and A3 are called "cross sections" in this report. These data were collected on the subgrade prior to installing mat, on the mat surface prior to starting traffic and at scheduled pass levels during traffic, and on the subgrade surface after panels were picked up. The locations of perpendicular lines A1, A2, and A3 were selected near the quarter-points of the test items to characterize the average performance while avoiding potential end

effects associated with boundary conditions at the ends of the test sections. Robotic total station elevation data were collected at 6-in. intervals on the subgrade. On the mat surface, data were collected at 1-ft intervals from 2 ft to 10 ft offset from the centerline and at 6-in. intervals up to 2 ft offset from the centerline (Figure 24).

Figure 23. Surveying the subgrade after completing trafficking.

Figure 24. Surveying an unloaded (left) and a loaded (right) cross section.

3.4.3 Loaded cross sections

In an attempt to measure the permanent deformation of the subgrade underneath the mat surface, a forklift carrying two 2,000-lb. lead weights was parked on the mat surface adjacent to each cross section, and

elevation data were once again recorded at the same intervals (Figure 24). The wheel load applied was approximately 6,000 lb. These data are noted as "loaded cross sections" in this report. The goal of the load application was to deflect the mat enough to contact the subgrade but not so much as to induce elastic deflections in the subgrade.

3.4.4 Elastic deflection

Elastic deflection was measured at the pass levels in Table 6 by taking robotic total station readings at the locations shown in Figure 22, both on the unloaded mat surface and immediately adjacent to the tire of the load cart parked on the same locations (Figure 25). The center of three panels and the end connector joint at three locations were specifically chosen to represent the least and most critical positions of the mat, respectively.

Figure 25. Elastic deflection measurement.

3.5 Failure criteria

The failure criteria established were either (1) 10 percent mat breakage or (2) the development of 1.25 in. of permanent surface deformation for the F-15E. These failure criteria were developed based upon previous testing of airfield matting and USAF requirements. Failure criteria values were recorded and monitored for compliance.

3.5.1 Mat breakage

Mat breakage percentages were calculated by dividing the area of the failed panel (or half-panel) by the total area influenced by the simulated traffic application in the assembled test item. For example, the total area influenced by Item A was 1,008 ft^2 (24 ft by 42 ft). Ten percent of this area is 100.8 ft^2, which is equal to the area of 4.2 12-ft panels (5 full-panels). Individual panels were considered failed if observed damage posed a significant tire hazard or caused instability of the load cart. Tire hazards were defined as damage that could not be reasonably maintained by simple field maintenance procedures. A typical example was a top skin tear in excess of 10, representing significant structural damage to the surface skin with sharp edges that might endanger an aircraft tire.

3.5.2 Permanent deformation

The permanent surface deformation limit of 1.25 in. was based on roughness limitations for the F-15E aircraft. An abrupt change in elevation or the development of a rut in the wheel path greater than the allowable values may exceed roughness limits. The rut depth limit is required, since many connecting taxiways and aprons intersect at a 90 deg angle, and crossing perpendicular to a preformed rut may cause an abrupt change in elevation, exceeding aircraft limits. Permanent surface deformation was determined from robotic total station elevation measurements of cross sections and centerline profiles. Each of the following data collection categories was analyzed for compliance with the failure criterion:

1. centerline profile deformation,
2. unloaded surface deformation, and
3. loaded surface deformation.

3.5.2.1 Centerline profile deformation

The difference in elevation one to two stations apart (1 ft to 2 ft apart) was analyzed from plots of the centerline profile data to determine whether an abrupt change in elevation reached failure limits during trafficking.

3.5.2.2 Unloaded surface deformation

The unloaded surface deformation was determined from data collected according to the procedures described in Section 3.4.2. The maximum deformation at each location was determined as the difference in elevation

from the average height of the elevated material on each side of the trough to the deepest point in the bottom of the trough. Measurements were averaged to obtain a single value for comparison to the failure criterion.

3.5.2.3 Loaded surface deformation

The loaded surface deformation was determined from data collected according to the procedures described in Section 3.4.3. The maximum deformation at each location was determined as the difference in elevation from the average height of the elevated material on each side of the trough to the deepest point in the bottom of the trough. Measurements were averaged to obtain a single value for comparison to the failure criterion.

4 Test Results

4.1 Mat behavior under traffic (visual observations)

The following sections describe all mat breakage and the behavior of the AM2 airfield mat. Figure 26 shows the layout of failed panels in each test item.

Figure 26. Layout of failed panels.

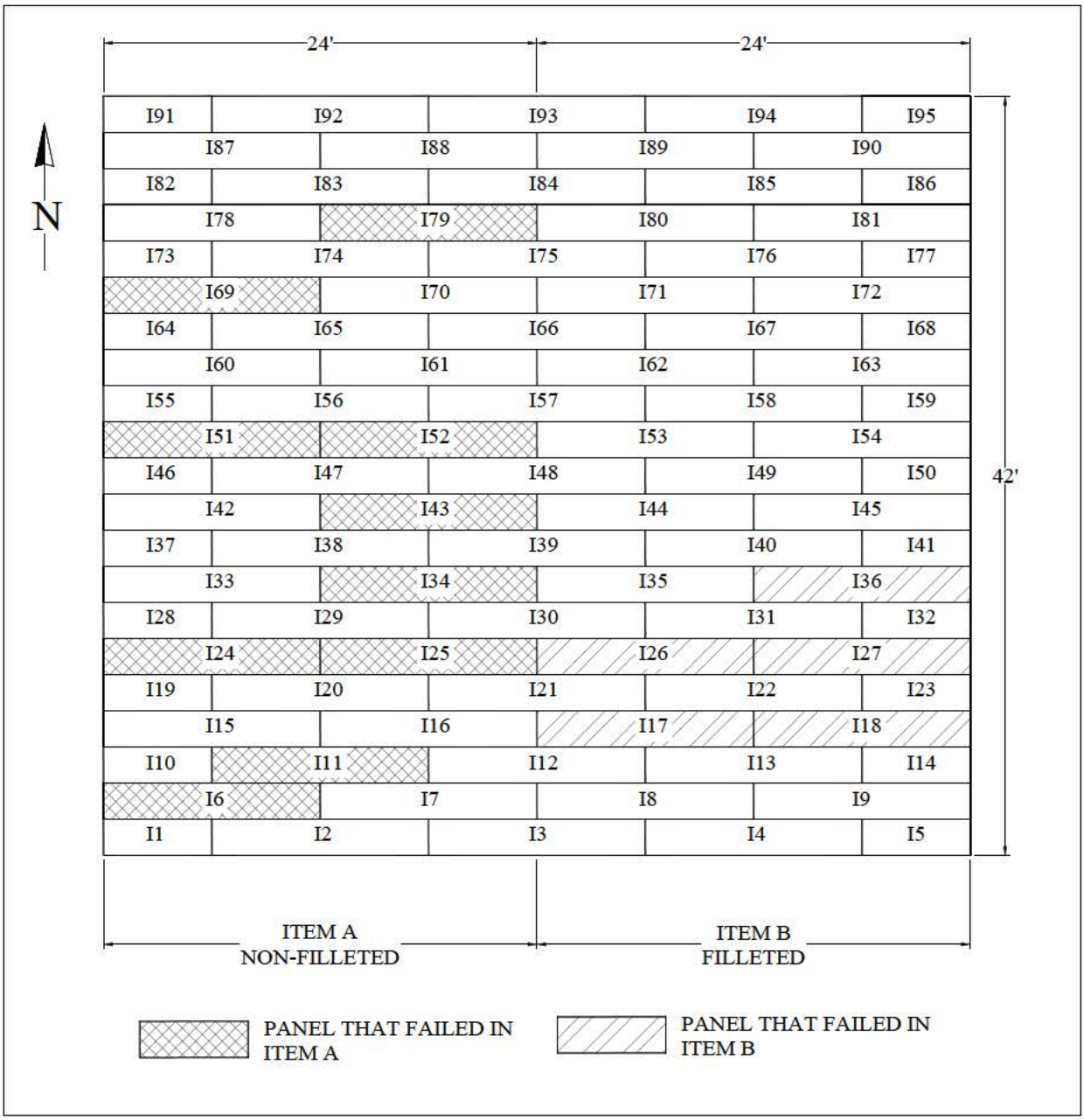

4.1.1 Item A

Trafficking of Item A began on September 23, 2014. The accumulation of mat damage and mat breakage throughout trafficking on Item A and after panels were removed from the subgrade surface is summarized in Table 7. Loaded deformation values during the test are also provided in Table 7. After 496 passes, only one panel had failed, equaling 2.4 percent of the test item. However, the loaded deformation on the mat surface reached 1.50 in., exceeding the permanent deformation criterion of 1.25 in. Therefore, Item A failed by permanent deformation. However, traffic was continued to capture additional information.

Table 7. Mat damage in Item A.

Pass number	Panel number	Description of damage	Cumulative failed panels	Cumulative mat breakage, %	Loaded deformation on mat surface (in.)
48	-	-	-	-	0.52
100	I-6	Lower overlap rail broke	1	2.4	
	I-7	0.19-in. corner curl	-	-	
112	-	-	-	-	0.70
240	-	-	-	-	0.97
420	I-7	Top skin tear along top flange of female hinge, 2.5 in. long	-	-	
496 *	I-7	Top skin tear length increased to 5 in. Cut for maintenance.	-	-	**1.51**
	I-6, I-52, I-51	0.25-in. corner curl	-	-	
	I-15, I-16, I-42, I-43, I-60, I-61, I-33, I-34, I-69, I-70, I-78, I-79, I-87, I-88	0.19-in. corner curl	-	-	
710	I-11	11-in.-long crack on surface, parallel to long dimension, about 2.5 in. offset from top flange of female hinge	2	4.8	
	I-69	Overlap end connector detached	3	7.1	
	I-6	Crack along weld that began at south edge, 2 in. long	-	-	
770	I-11	Crack length increased to 18 in.	-	-	
	I-7	Top skin tear length increased to 9 in. Cut for maintenance.	-	-	

Pass number	Panel number	Description of damage	Cumulative failed panels	Cumulative mat breakage, %	Loaded deformation on mat surface (in.)
	I-15, I-16, I-25, I-33, I-34, I-42, I-43, I-51, I-52, I-60, I-61	0.25-in. corner curl. Corner curl developed minor cracking on surface	-	-	
	I-24	Crack along weld that began at south edge, 2.5 in. long	-	-	
	I-25	Upper underlap rail broke	4	9.5	
807	I-25	Top skin tear along top flange of female hinge, 5 in. long. Cut for maintenance.	-	-	
923	I-51	Overlap end connector detached	5	11.9	
	I-6	5-in.-long top skin tear, parallel to female hinge. Top skin lifted a width of 2 in.	-	-	
	I-34	Top skin tear 4.5 in. -long along top flange of female hinge. Cut for maintenance	-	-	
	I-24	Southeast corner of top skin broke	-	-	
	I-25	Top skins tear length increased to 17 in.	-	-	
1,008	I-24	10-in.-long crack, parallel to female hinge. Top skin lifted a width of 2.5 in.	6	14.2	2.45
	I-34	Upper underlap rail broke. Top skin tear length increased to 15 in.	7	16.6	
	I-52	Upper underlap rail broke. Top skin tear 13 in. long along top flange of female hinge	8	19.0	
	I-79	Upper underlap rail broke	9	21.4	
	I-43	Top skin tear 6 in. long along top flange of female hinge. Separation noted at joint with I-42.	-	-	
	I-33, I-42, I-51, I-15, I-16	Severe corner curl	-	-	
	I-6	Top skin tear length increased to 11 in.	-	-	
	I-7	Top skin tear lifted a width of 2 in.	-	-	
	I-11	Crack length on surface increased to 36 in.	-	-	

Pass number	Panel number	Description of damage	Cumulative failed panels	Cumulative mat breakage, %	Loaded deformation on mat surface (in.)
Post Test (1,008)	I-83	10-in.- long crack along face of female hinge	-	-	
	I-78, I-15	Crack at weld of overlap end connector from top surface to bottom surface	-	-	
	I-74	5-in.-long hairline crack along face of female hinge	-	-	
	I-69	Crack below southeast corner of top flange of female hinge, 7.5 in. long	-	-	
	I-70, I-16	Hairline crack at weld of underlap end connector	-	-	
	I-42	Lower overlap rail broke length of 9 in., starting at female hinge edge. Crack at end connector weld from top surface to bottom surface.	-	-	
	I-43	Upper underlap rail broke length of 17 in., starting at male hinge edge.	10	23.8	
	I-33	Crack at end connector weld from top surface to bottom surface that extended 1 in. on bottom skin	-	-	
	I-29	Bottom flange of female hinge tore a length of 20 in. Hairline crack 5 in. long along face of female hinge	-	-	
	I-11	Crack along face of female hinge, 50 in. long. Crack on bottom skin, 40 in. long, 2.5 in. from edge of bottom flange of female hinge.	-	-	
	I-6	Crack at end connector weld from top surface to bottom surface that extended 3 in. on bottom skin	-	-	
	I-2	Crack along male hinge, 9 in. long	-	-	

* Item A failed by permanent deformation > 1.25 in.

The most common mat breakage was broken upper underlap rails (Figure 27). When a rail failure occurred, separation was noted at the adjoining panels as the load cart passed over the joint. Upper underlap rail failure was confirmed when a crack could be seen at the rail from the

surface. Lower overlap rail failure was also documented. Since the lower overlap rail was not visible from the surface, breakage at this location was confirmed when (1) separation was observed at a joint but the upper underlap rail was noticeably intact or (2) mat panels were removed from the subgrade surface.

Figure 27. Broken upper underlap rail I-79 (left) and I-25 (right).

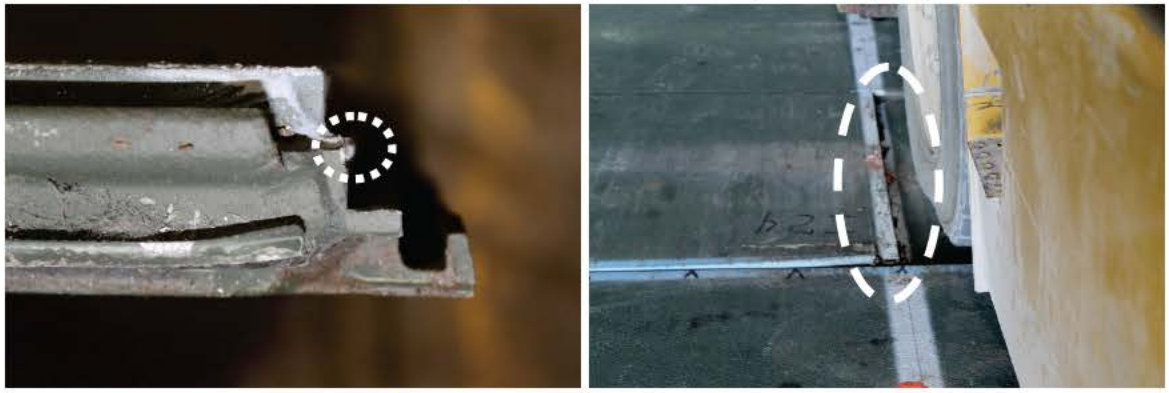

Top skin tears occurred in some panels with their end connector in the traffic area. A top skin tear typically began at (or near) the south edge of the end connector weld and propagated along the top flange of the female hinge. Examples are shown in Figure 28. In two panels, a crack developed along the weld and extended about 2 in. before continuing its propagation parallel to the female hinge. An example is shown in Figure 29 for Panel I-6. Top skin corner curls were also very common. These occurred at the south corner of panels with their end connector along the centerline. They usually occurred before top skin tearing was noted. If a top skin tear reached a point where it was posing a risk to the load cart tire, the loose skin was removed for maintenance. Skin tears greater than 10 in. were difficult to maintain, and traffic had to be stopped frequently for maintenance. Therefore, if the length of a top skin tear reached more than 10 in., the panel was considered failed. Corner curls that also posed a risk to the tire were hammered down. Panels I-69 and I-51 both failed because the end connector along the centerline detached (Figure 30). From the surface, this was obvious from cracking observed along the length of the weld. Panel I-11 failed as a result of skin tearing at the center, near the female hinge. This likely occurred adjacent to one of the core vertical stiffeners (Figure 31).

Mat breakage failure was reached after 923 passes when a total of 5 panels were documented as failed. After 1,008 passes, the extent of damage in the lane was causing instability to the load cart and posing a risk to the tire.

Figure 28. Top skin tear at I-7 (left) and I-34 (right).

Figure 29. Top skin tear at I-6.

Figure 30. Detached end connector at I-51 (left) and I-69 (right).

Figure 31. Crack on bottom (left) and top (right) surface of I-11.

Trafficking was concluded on Item A and initiated on Item B. After panels from Item A were removed from the subgrade surface, some panels with their center along the traffic lane had developed cracking along the face of the female hinge. Others were noted to have cracks at the weld of the end connector that could be observed only after picking up the panels (Figure 32).These cracks indicated the initiation of end connector detachment but did not render a panel failed, since the surface was still safe and usable. Two panels had partially cracked rails (I-42 and I-43). Since the length of breakage at the rail of I-43 was greater than 12 in., the panel was considered failed, increasing mat breakage to 23.8 percent.

Figure 32. Crack at weld and broken lower overlap rail at I-42.

4.1.2 Item B

Traffic on Item B began on September 26, 2014. The accumulation of mat damage and mat breakage throughout trafficking on Item B and after panels were removed from the subgrade surface is summarized in Table 8. Loaded deformation values during the test are also provided in Table 8. After 1,008 passes, the loaded deformation on the mat surface reached 1.81 in., exceeding the permanent deformation criterion of 1.25 in. Therefore, Item B failed by permanent deformation. However, traffic was continued to capture additional information.

Table 8. Mat damage in Item B

Pass number	Panel number	Description of damage	Cumulative failed panels	Cumulative mat breakage, %	Loaded deformation on mat surface (in.)
112	-	-	-	-	0.51
240	All panels with joint along centerline	0.19-in. corner curl	-	-	0.74
496	I-89, I-90, I-80, I-81, I-71, I-62, I-53, I-44, I-35, I-36	Minor cracking on surface of corner curl	-	-	1.06
962	I-27	Top skin tear along top flange of female hinge, 5 in. long	-	-	
	I-26	Severe corner curl with minor cracking on surface	-	-	
	I-35, I-44, I-53, I-45, I-36, I-54, I-62, I-63	0.25-in. corner curl	-	-	
1,008**	I-27	Top skin tear length increased to 9 in. Cut for maintenance	-	-	**1.81**
	I-26	Top skin tear along top flange of female hinge, 5 in. long. Cut for maintenance	-	-	
1,176	I-18	Upper underlap rail broke. 5-in.-long skin tear along top flange of female hinge. Cut for maintenance.	1	2.4	
	I-17	Severe corner curl	-	-	
1,186	I-18	Top skin tear along top flange of female hinge, 19 in. long. Cut for maintenance	-	-	

Pass number	Panel number	Description of damage	Cumulative failed panels	Cumulative mat breakage, %	Loaded deformation on mat surface (in.)
	I-13	Male hinge cracked and bent	-	-	
	I-26	Top skin tear along top flange of female hinge, 12.5 in. long. Cut for maintenance.	2	4.8	
	I-27	Top skin tear along top flange of female hinge, 15 in. long. Cut for maintenance.	3	7.1	
	I-35, I-36, I-44, I-45, I-53, I-62, I-80, I-89	Severe corner curl	-	-	
1,191	I-17	Top skin tear along top flange of female hinge, 9 in. long. Cut for maintenance.	-	-	
1,210	I-18	Top skin tear length increased to 24 in. Cut for maintenance	-	-	
	I-17	Top skin tear length increased to 15 in. Cut for maintenance	4	9.5	
1,232*	I-26	Top skin tear length increased to 14 in. Cut for maintenance	-	-	2.20
	I-22	Bottom flange sheared at connection with I-18	-	-	
1,520	-	-	-	-	2.65
1,760	I-53, I-62	Crack developed on surface of overlap end connector, starting at north edge. About 1 to 1.5 in. long	-	-	
1,970	I-80, I-44, I-35, I-26, I-89	Crack developed on surface of overlap end connector, starting at north edge. About 1 to 1.5 in. long	-	-	
2,052	I-36	Top skin tear along top flange of female hinge, 5 in. long. Cut for maintenance.	-	-	
2,056	I-36	Upper underlap rail broke. Top skin tear increased to 11.5 in. long.	5	11.9	

Pass number	Panel number	Description of damage	Cumulative failed panels	Cumulative mat breakage, %	Loaded deformation on mat surface (in.)
	I-8	Crack developed on surface of overlap end connector, starting at north edge. About 1 in. long	-	-	
	I-27	Top skin tear length increased to 29 in. Cut for maintenance	-	-	
	I-26	Top skin tear length increased to 30 in. Cut for maintenance	-	-	
	I-36	Top skin tear length increased to 16 in. Cut for maintenance	-	-	
	I-89	Length of crack on surface of overlap end connector increased to 2 in.	-	-	
2,060	-	-	-	-	3.38
Post Test (2,060)	I-94	Crack along face of female hinge, 14 in. long	-	-	
	I-80, I-71	Hairline crack at weld of overlap end connector	-	-	
	I-81, I-45, I-27	Hairline crack at weld of underlap end connector	-	-	
	I-76	Crack along face of female hinge, 10 in. long	-	-	
	I-67	Hairline crack at face of female hinge, 7 in. long	-	-	
	I-62, I-35, I-36	Crack at weld of end connector from top surface to bottom surface	-	-	
	I-58	Crack along face of female hinge, 15.5 in. long	-	-	
	I-54	Upper underlap rail broke length of 3 in., starting at female hinge. Hairline crack at weld.	-	-	
	I-53	Minor cracking at top of weld of end connector	-	-	
	I-44	Crack at weld of end connector from top surface to bottom surface that extended 1.75 in. on bottom skin	-	-	

Pass number	Panel number	Description of damage	Cumulative failed panels	Cumulative mat breakage, %	Loaded deformation on mat surface (in.)
	I-40	Crack along face of female hinge, 11.5 in. long	-	-	
	I-31	Bottom flange of female hinge tore length of 3 in. Hairline crack along face of female hinge, 9 in. long	-	-	
	I-22	Bottom flange of female hinge tore length of 22 in.	-	-	
	I-8	Crack at weld of end connector from top surface to bottom surface that extended 2 in. on bottom skin	-	-	

*Placed metal plate above I-17 and I-18 to continue traffic

** Item B failed by permanent deformation > 1.25 in.

Typical failure mechanisms were top skin tearing greater than 10 in. and upper underlap rail breakage. The most common damage was minor top skin tearing and corner curls. The male hinge of Panel I-13 developed cracking that was observed from the surface due to the severe skin tear at joining panel I-18 (Figure 33). After 1,232 passes, the rail failure and skin tear at I-18 were posing serious risk to the load cart tire. Since it was important to continue traffic until mat breakage failure was achieved, a metal plate was placed above Panels I-17 and I-18 to bridge over the damaged area (Figure 34). After 1,760 passes, cracking was noted on the surface of the overlap end connector of a few panels in the traffic area (Figure 35). Each crack was located just above the interface of the overlap/underlap joint and was less than 1.5 in. long. Their length hardly increased for the remainder of the test.

Mat breakage failure was reached after 2,056 passes when a total of 5 panels were documented as failed. Traffic was concluded on Item B after 2,060 passes, and the panels were removed from the test subgrade. After panels were picked up, a few with their center along the traffic lane had developed cracking along the face of the female hinge. More than 8 panels were noted to have cracks at the weld of the end connector that could be observed only after picking up the panels (Figures 36 and 37). One panel was partially broken at the upper underlap rail, but the length of cracking was 3 in. (much less than half the length of the rail) and was therefore not considered failed.

Figure 33. Skin tear and upper underlap rail failure at I-18.

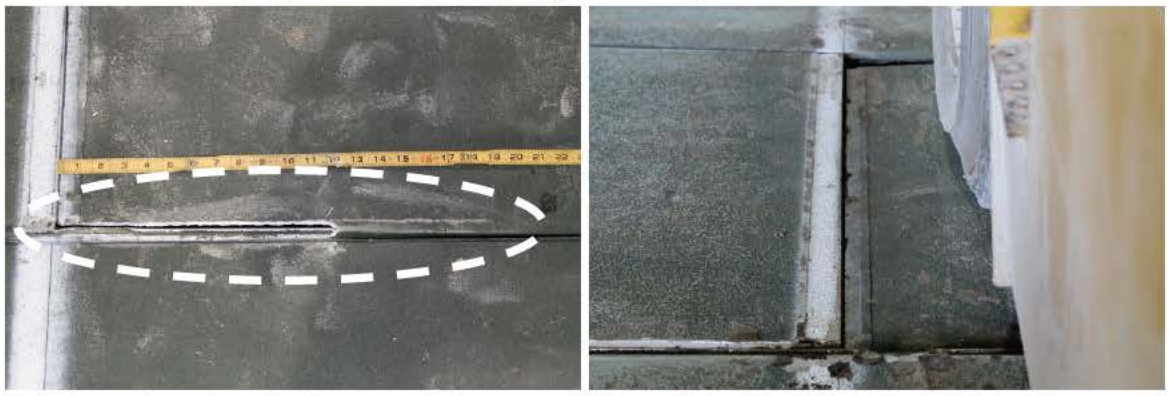

Figure 34. Metal plate placed above I-17 and I-18.

Figure 35. Crack at upper overlap rail of I-62 (left) and I-89 (right).

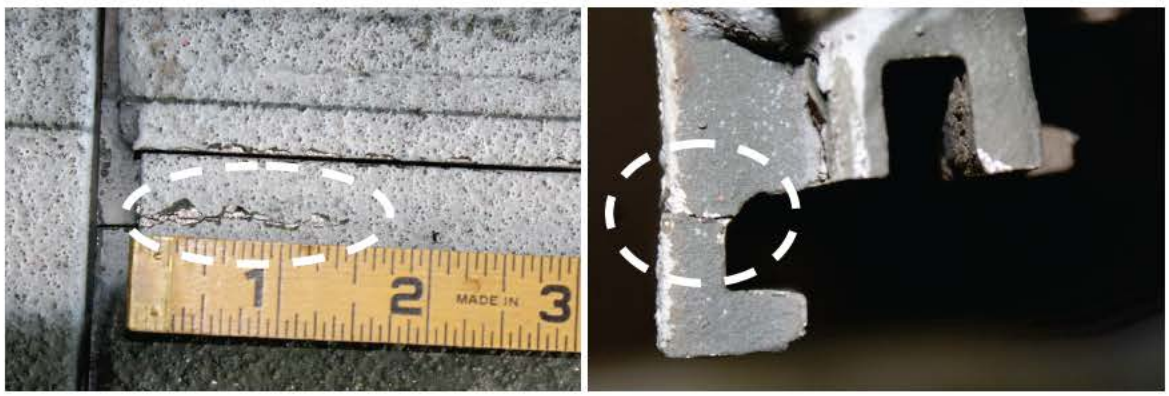

Figure 36. Crack at weld of I-62.

Figure 37. Cracked upper underlap rail and hairline crack at weld of I-54.

4.2 Permanent deformation

To show only the changes that occurred because of trafficking, the pre-traffic data were subtracted from all subsequent data collected after trafficking began, in order to normalize the data. The discussions and results that follow are based on normalized data. Plots of the centerline profile data, as determined from robotic total station recordings are shown in Figures 38 through 41.

In Item A, stations 2 to 4 and stations 10 to 12 were areas of panel end connector rail failure and are represented as deep depressions in the subgrade (Figures 38). These were disregarded when analyzing the profile since they were associated with mat breakage and not necessarily with the system's ability (or inability) to prevent excessive roughness. As shown in Figures 39 and 41, the same is true for stations 14 to 16 in Item B. Buildup of material also occurred beneath the plate placed above panels I-17 and I-18 (about stations 6 to 8); therefore, the change in elevation from stations 8 to 10 in Figure 39 would appear to be the maximum roughness value. This was also disregarded when analyzing the subgrade profile, since it was associated with the metal plate placed above the mat surface and not with the performance of the system itself.

Figure 38. Subgrade centerline profile of Item A after 1,008 passes.

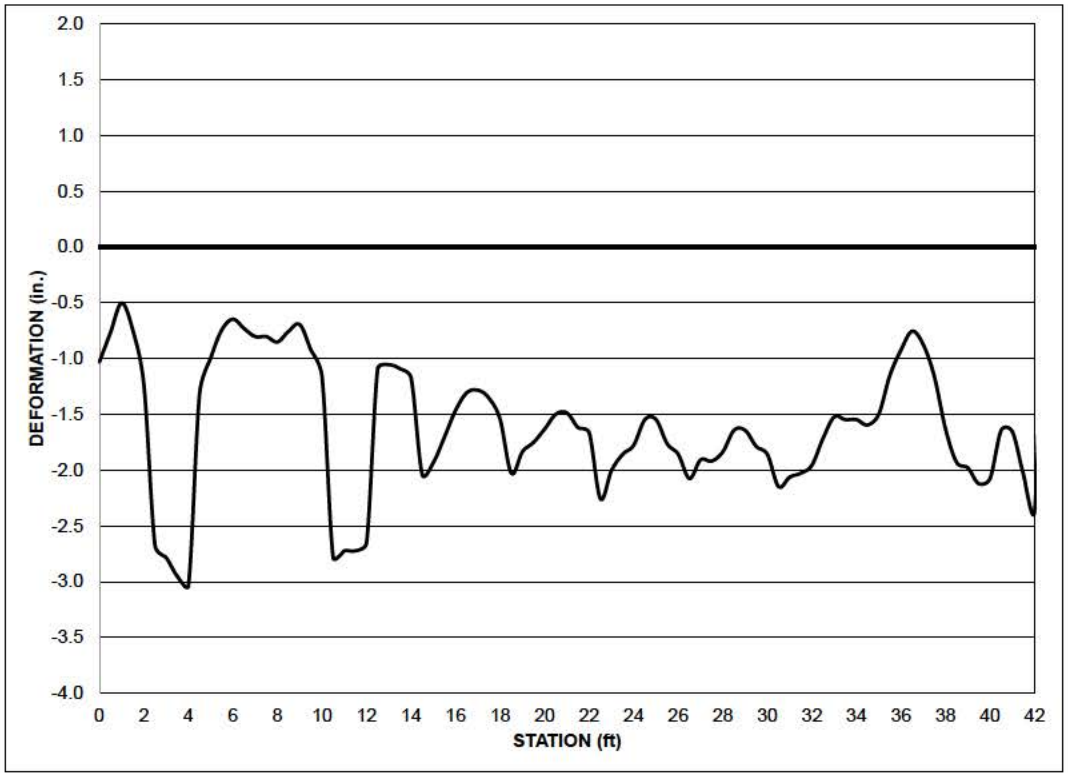

Figure 39. Subgrade centerline profile of Item B after 2,060 passes.

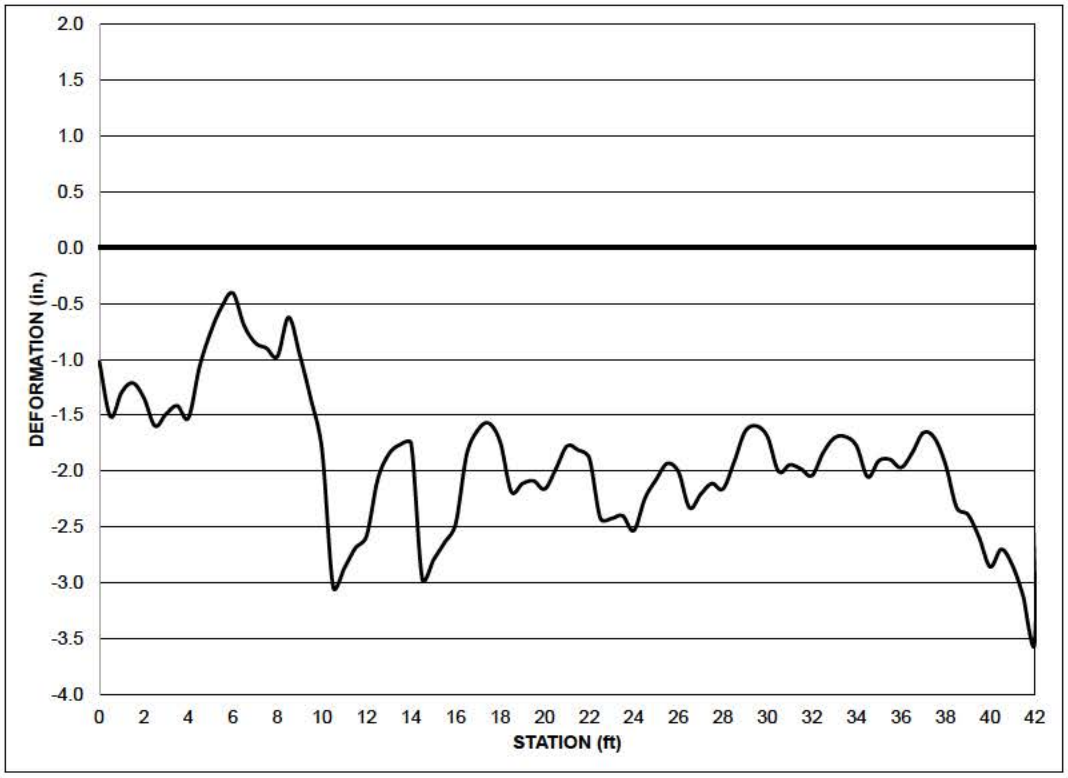

Figure 40. Centerline profile on the mat surface of Item A at different pass levels.

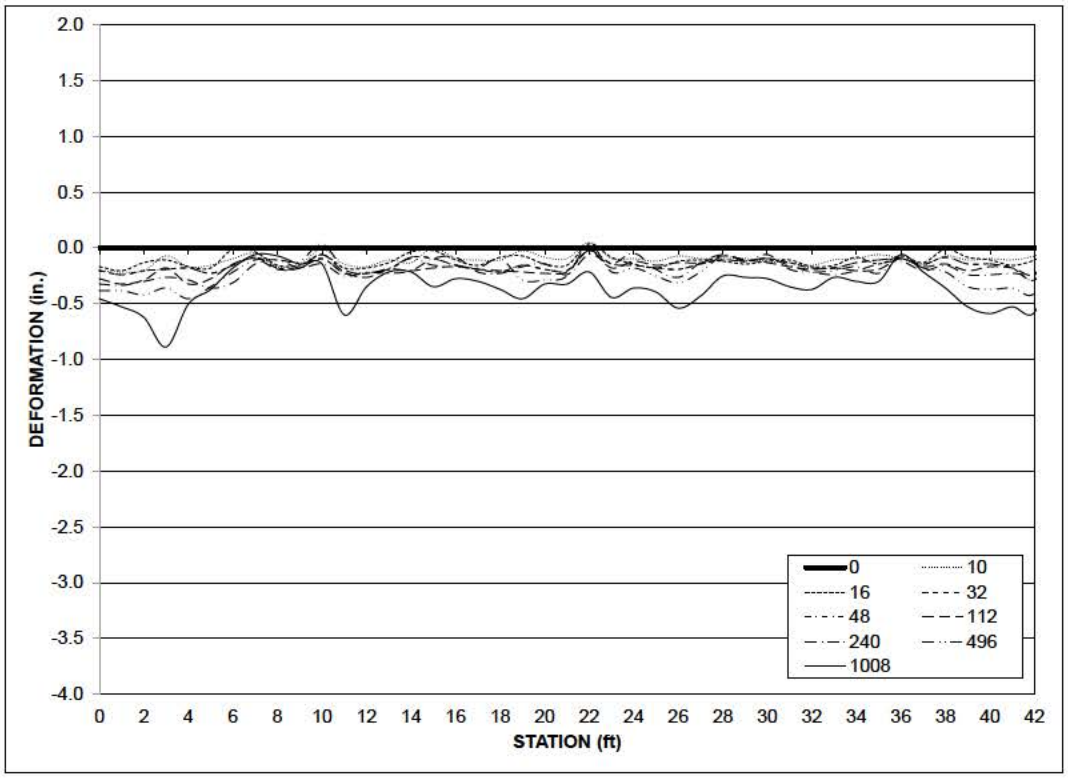

Figure 41. Centerline profile on the mat surface of Item B at different pass levels.

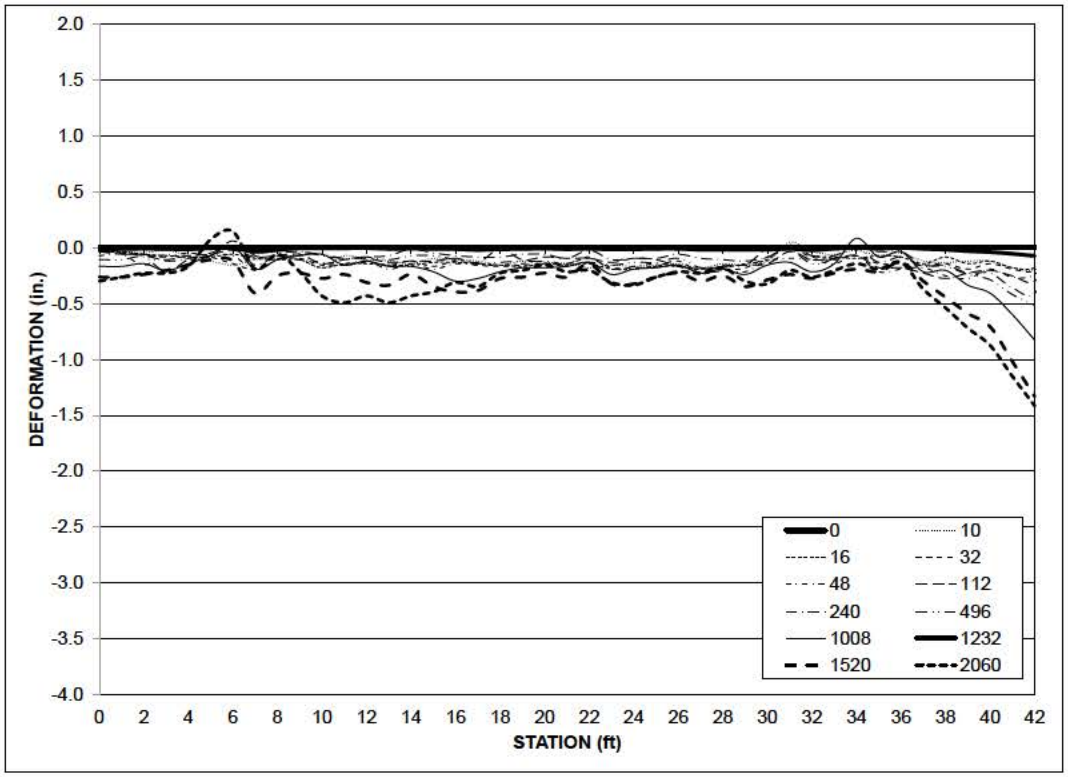

Plots of the average cross-section elevation data, collected along lines A1, A2, and A3 for each test item, are shown in Figures 42 through 47. Table 9 summarizes important deformation values determined from all the plots for comparison to the failure criterion.

4.3 Elastic deflection

The difference between the loaded (immediately adjacent to the tire of the load cart) and the unloaded elevation at the locations shown in Figure 22 represents the elastic deflection, or rebound, of the mat and the subgrade at each location. The measurements determined from readings taken at the center of three panels were averaged to give a final elastic deflection value. The same was done for measurements determined from readings taken at three joints. The average of these two values was also calculated. One number was reported for each condition at each pass level in Table 6. The results are shown in Figures 48 and 49 for Item A and Item B, respectively.

Figure 42. Average deformation on the subgrade of Item A after 1,008 passes.

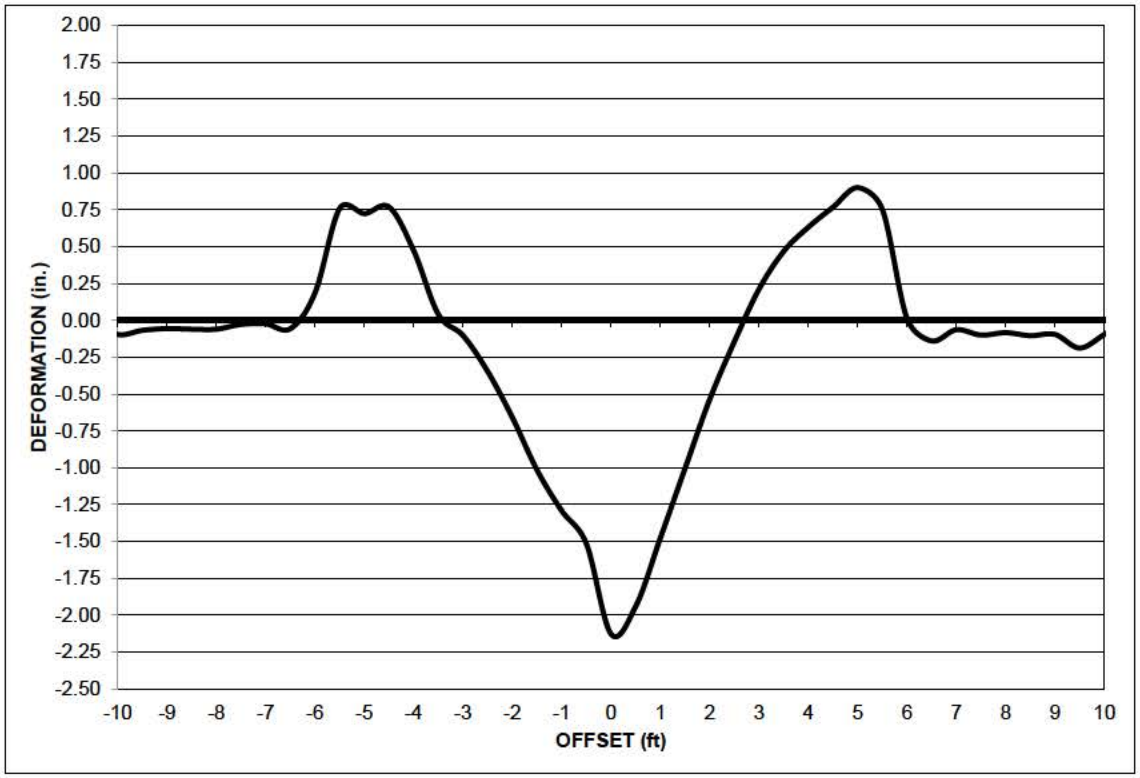

Figure 43. Average deformation on the subgrade of Item B after 2,060 passes.

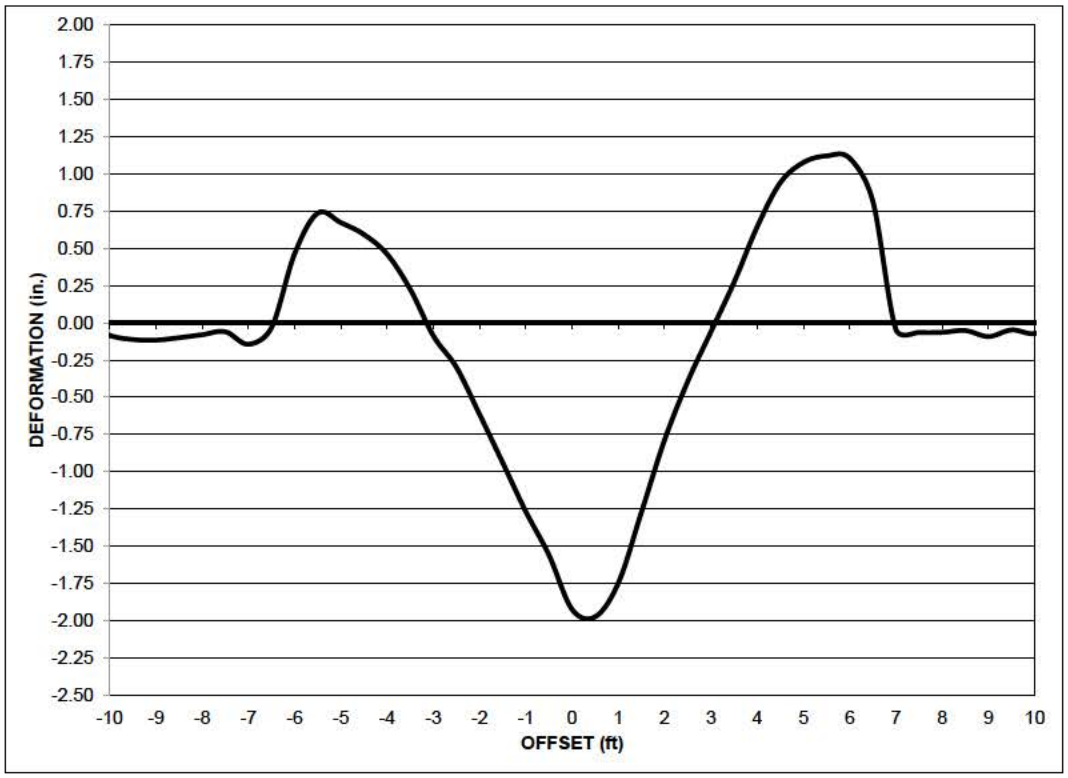

Figure 44. Average deformation on the unloaded mat surface of Item A at different pass levels.

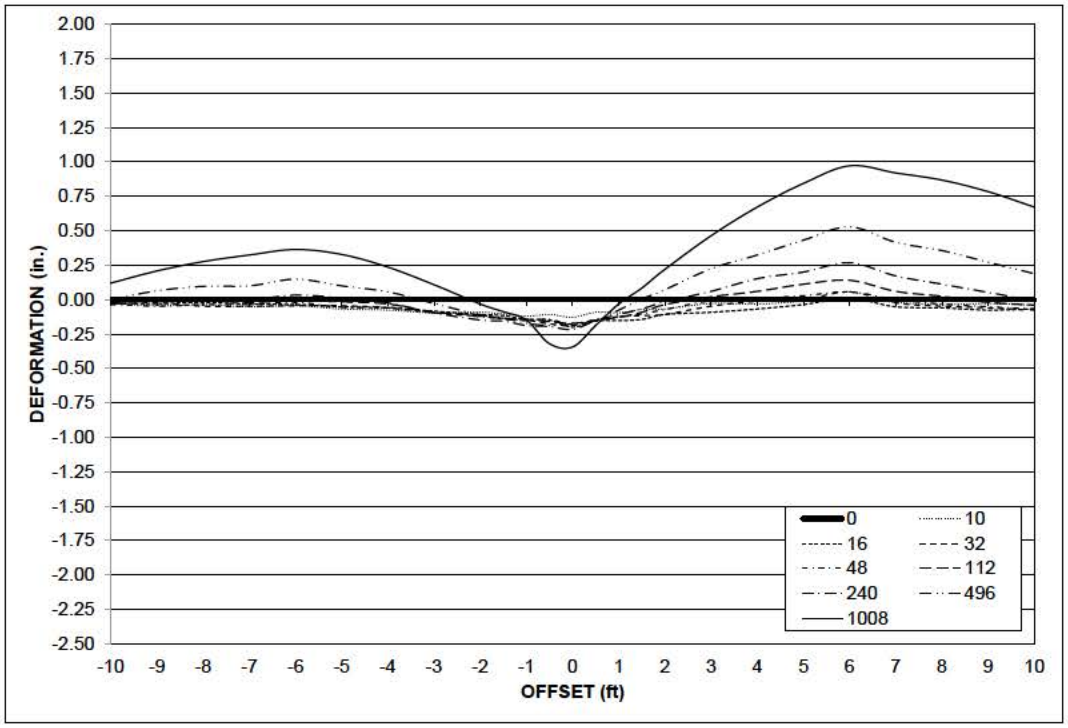

Figure 45. Average deformation on the unloaded mat surface of Item B at different pass levels.

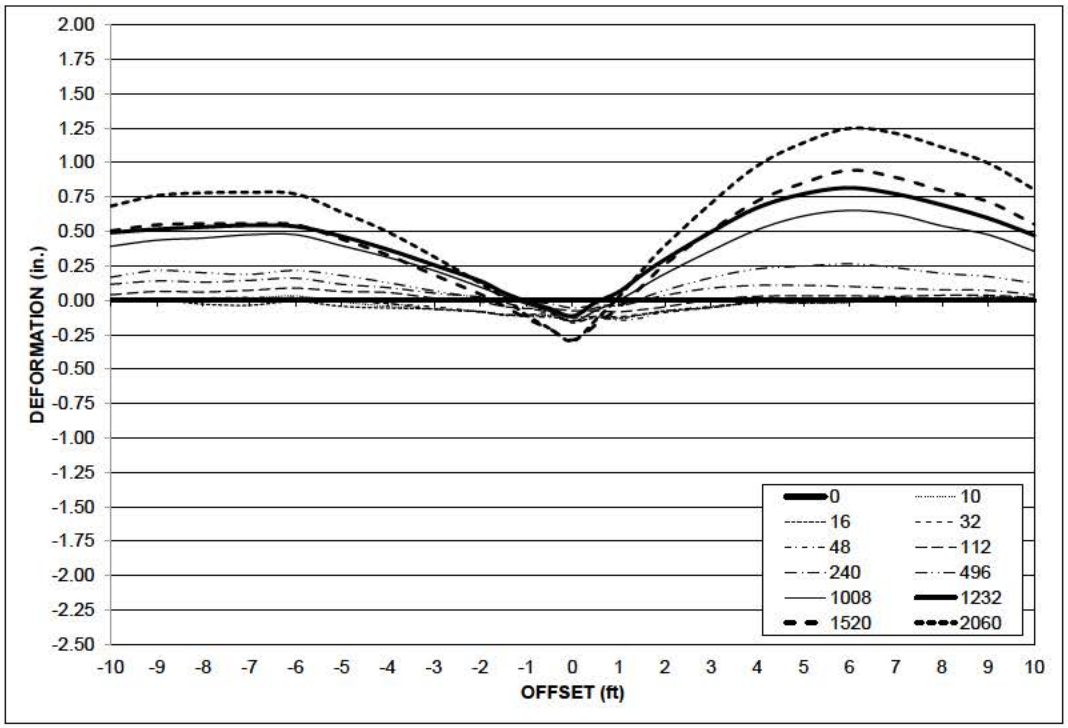

Figure 46. Average deformation on the loaded mat surface of Item A at different pass levels.

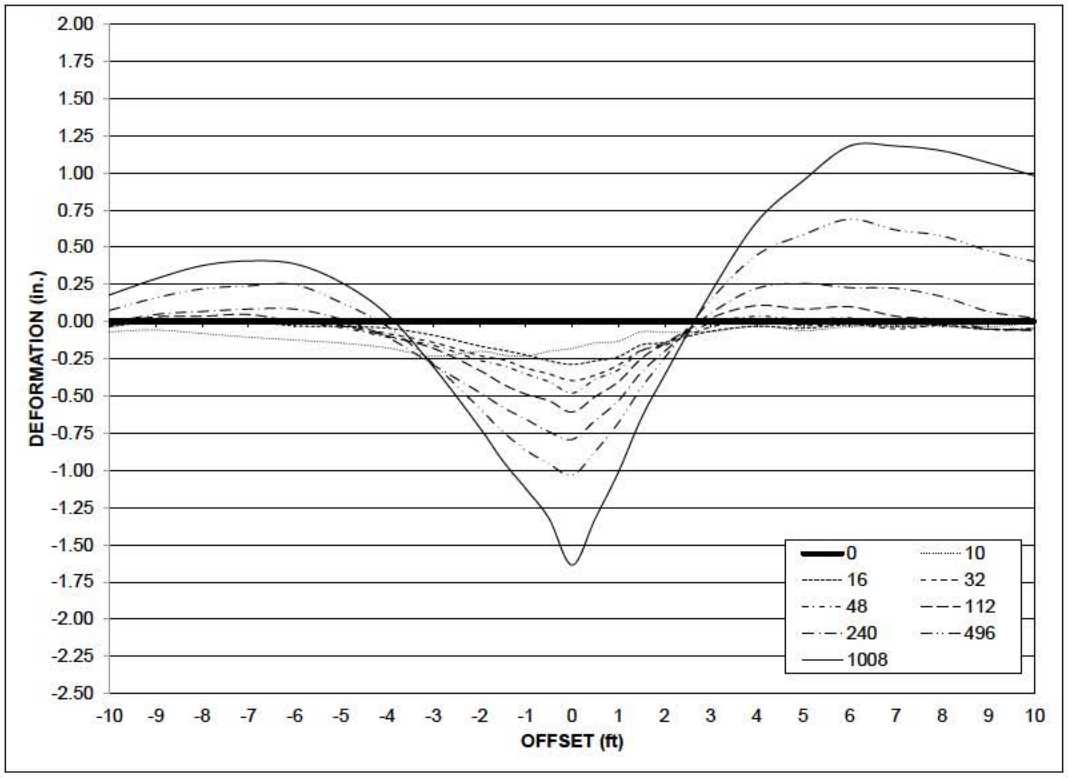

Figure 47. Average deformation on the loaded mat surface of Item B at different pass levels.

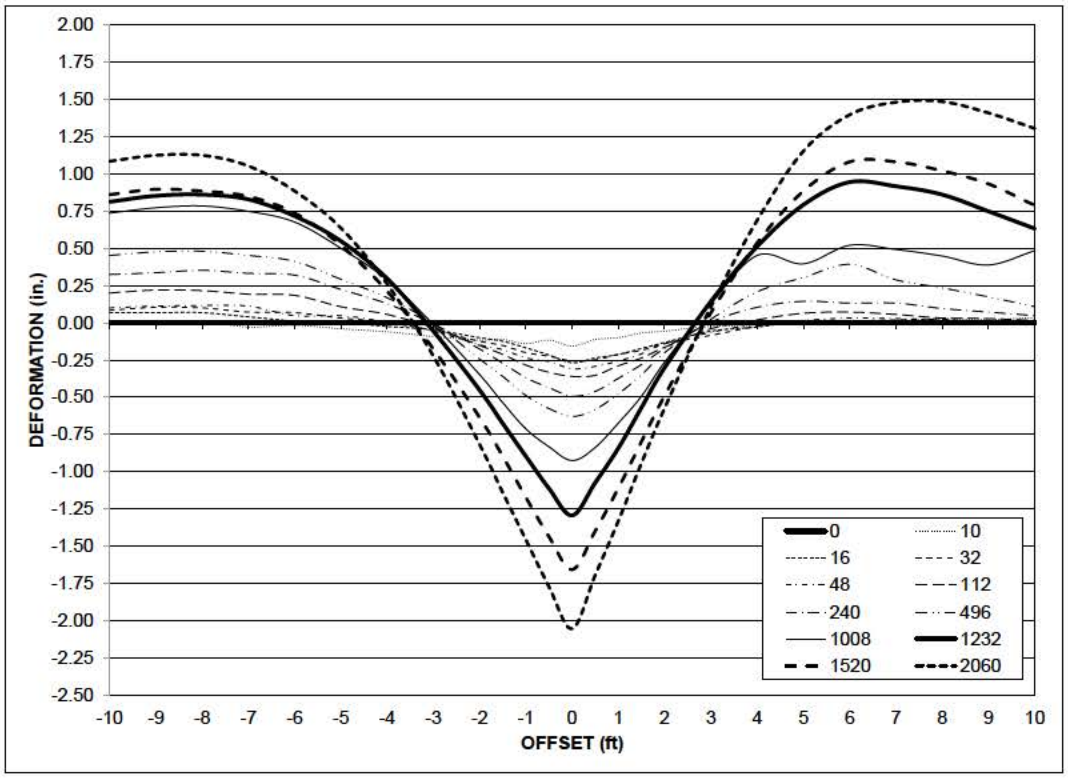

Table 9. Permanent deformation values.

Test Item	Item A		Item B		
Pass Number	496	1,008	496	1,008	2,060
Subgrade Profile Max Abrupt Change in Elevation (in.)	-	0.84	-	-	0.60
Mat Surface Profile Max Abrupt Change in Elevation (in.)	0.32	0.29		0.08	0.12
Subgrade Permanent Deformation (in.)	-	2.97	-	-	2.98
Loaded Deformation on Mat Surface (in.)	1.51*	2.45	1.06	1.81*	3.38
Unloaded Deformation on Mat Surface (in.)	0.56	1.05	0.36	0.72	1.34

*Failed by exceeding 1.25-in. limit

Figure 48. Elastic deflection in Item A.

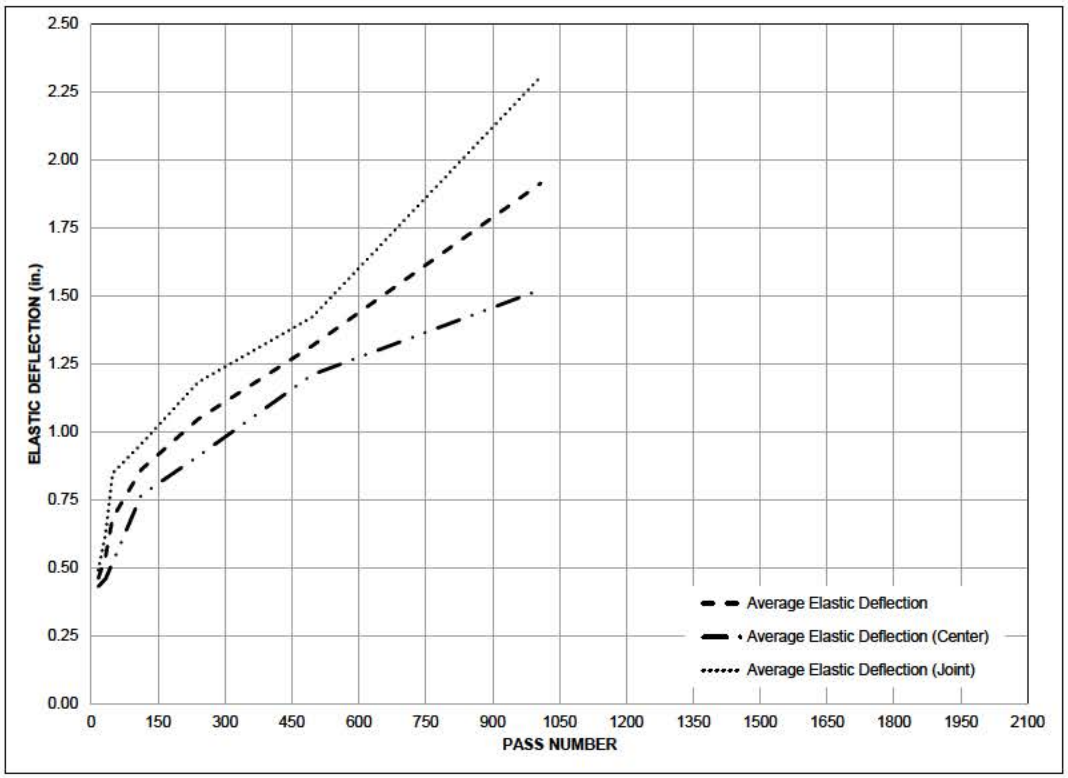

Figure 49. Elastic deflection in Item B.

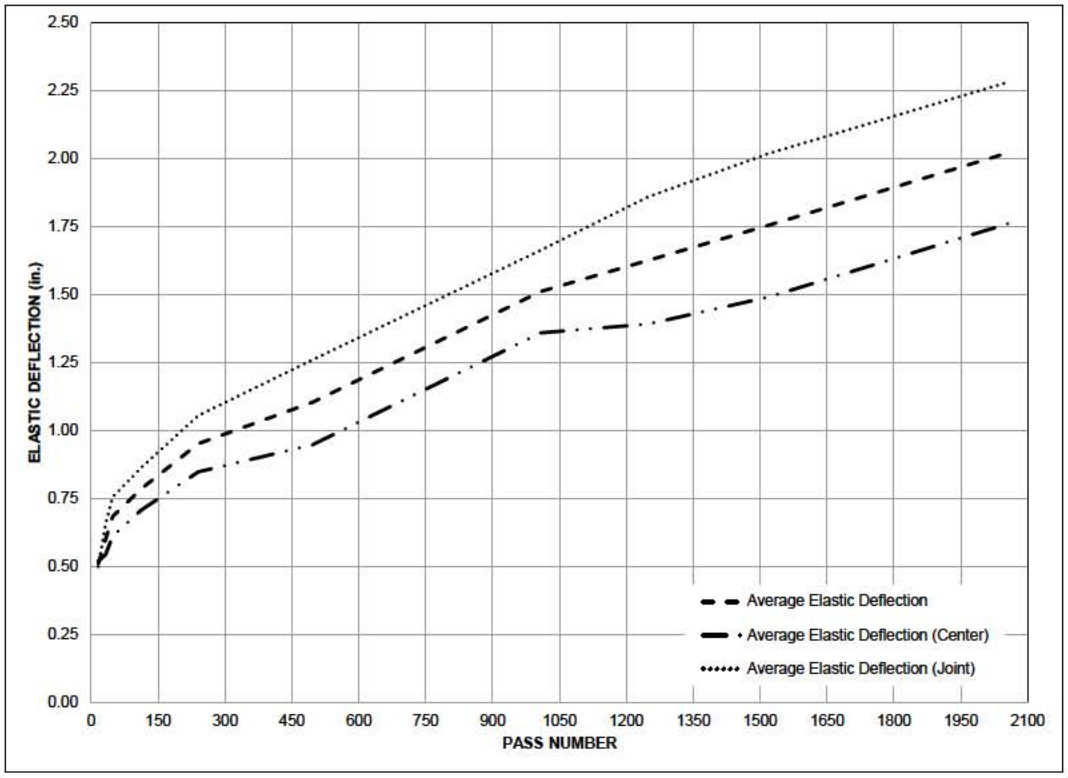

5 Analysis of Results

5.1 Mat breakage

A summary of the progression of mat breakage for each test item is shown in Figure 50 for comparative purposes. Item A and Item B were able to sustain 923 passes and 2,056 passes, respectively, before failure by mat breakage. Two important things to note from Figure 50 are (1) panel failures in Item B started to occur about 250 passes after Item A was rated as failed and (2) at the end of each test, percent mat breakage in Item A was twice the amount noted in Item B. A comparison of the number of occurrences of the different failure mechanisms in each test item is provided in Table 10. Mat breakage in both test items was typical and similar to that reported by Rushing and Tingle (2007), Rushing and Torres (2007), Rushing et al. (2008), Rushing and Mason (2008), and Garcia and Rushing (2013) in AM2 when trafficked over weak subgrade conditions. End connector rail failures were the most common mechanism of mat breakage reported by these authors.

Figure 50. Comparison of percent mat breakage.

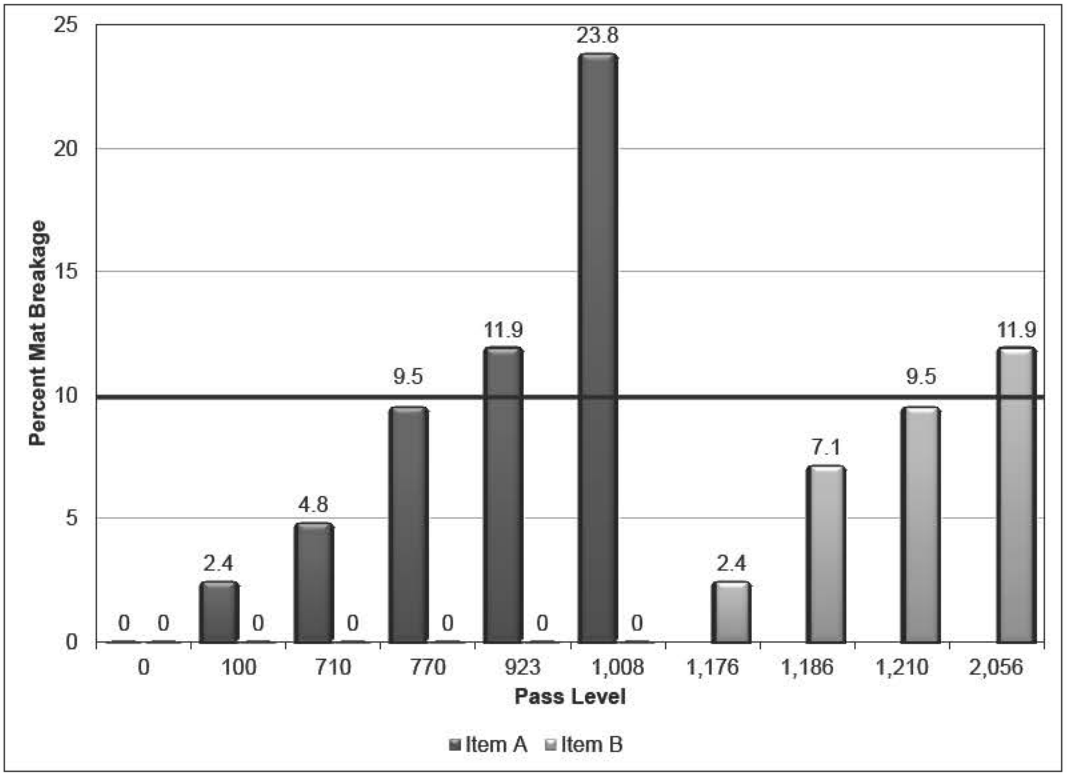

Table 10. Comparison of mat failure mechanisms.

Failure type	Number of panels	
	Item A	Item B
Broken upper underlap rail	5	2
Broken lower overlap rail	1	-
Top skin tear >10 in.	1	3
Top skin cracking at center	1	-
Detached end connector	2	-

It is obvious from the level of mat breakage and the number of occurrences of rail failures in Item A that the lack of filleted corners in the locking bar channel greatly decreases the performance life of AM2. The inclusion of the fillet was able to decrease stress concentrations in those areas, thus improving the fatigue life by inhibiting crack incubation from occurring at low cycles. With the filleted design, the critical damage location after a larger number of cycles began to shift from the upper underlap/lower overlap rails to the upper overlap rail, above the interface with the upper underlap rail of a connecting panel (Figure 35). This has not been documented for AM2 tests on soft soils. Most panels with end connectors along the traffic lane were noted to have developed cracking at this location and at the end connector weld. Although these did not increase in length to render a panel failed, it seems that after a larger number of load cycles, high stress concentrations developed at the upper overlap rail. This is consistent with the stress conditions shown in Figure 2b. Since improvement was noted with the filleted design in terms of rail breakage, changes could be made to the upper overlap rail to further increase fatigue life of the joint.

5.2 Permanent deformation

5.2.1 Centerline profile

The centerline profiles for the post-traffic subgrade and the surface of the mat at various traffic intervals were analyzed to determine whether the roughness criteria were exceeded. The maximum values for the subgrade and mat surface of both test items were all below the 1.25-in.-deep maximum value established for F-15E traffic. Therefore, both mat designs performed adequately in preventing excessive roughness from occurring. Similar results were reported by authors listed in Table 1 for previous evaluations of AM2 Mod 5 under F-15E traffic.

5.2.2 Cross sections

The permanent deformation on the subgrade, the loaded mat surface, and the unloaded mat surface was analyzed to determine whether the deformation criteria were exceeded. Item A failed by exceeding the permanent deformation limit of 1.25 in. after 496 passes on the loaded mat surface. Item B failed for the same reason after 1,008 passes. The subgrade deformation at the end of each test also exceeded the criterion in both test items. Since the subgrade surface deformation was determined after the mat panels were removed, the number of passes at which the 1.25-in. rut was developed in each test item could not be determined. Therefore, failure was assumed at pass 496 and 1,008 for Item A and Item B, respectively, even if the subgrade surface exceeded the limit beforehand. The rate of deformation on the loaded surface of Item A was nearly twice as fast as that measured on Item B.

5.3 Elastic deflection

Historically, elastic deflection measurements were used to monitor performance of mat systems, but were not used for mat system fatigue failure criteria. Average elastic deflection of the mat and subgrade increased throughout testing for both test items. The rate of increase was higher in Item A than in Item B. The elastic deflection reached approximately 2.25 in. for both test items, but this value was reached in Item A at half the number of passes that were sustained by Item B before reaching the same value. Assuming that the elastic deflection of the subgrade remained nearly constant throughout trafficking, the increase in the total elastic deflection of the mat and subgrade indicates that the air gap beneath the mat increased as deformation occurred in the subgrade surface. Since permanent deformation of the loaded mat surface in Item A occurred at a faster rate than in Item B, the elastic deflection then also increased at a higher rate. As expected, the average elastic deflection at the joints was higher throughout testing than at the center of panels, but the curves remained approximately parallel. Therefore, the rate of increase in elastic deflection was about the same at both locations, but the actual measured deflection was obviously higher at the joints.

6 Conclusions and Recommendations

6.1 Conclusions

The purpose of this effort was to conduct full-scale tests of the AM2 mat system under simulated F-15E traffic when installed over a subgrade with a CBR of 6. Recent investigations showed that the manufacturer's drawing of the extrusion die for the AM2 end connector inadvertently omitted filleted corners in critical stress locations in the locking bar channel. The die was recently corrected after an unknown period of producing the non-filleted design. Therefore, a corrected production version of AM2 was tested side-by-side with a section of AM2 having the non-filleted corners to compare their performance in terms of allowable passes to failure. Permanent deformation and mat breakage were monitored in each test item. The results of the tests were used to determine whether a reduction in performance was caused by the improper die.

The following conclusions were derived from accelerated traffic testing of the AM2 airfield matting system conducted September-October 2014:

- The AM2 panels produced without the filleted corners in the locking bar channel were able to withstand 496 passes before failure by permanent deformation and 923 passes before failure by mat breakage.
- The AM2 panels with the filleted corners in the locking bar channel were able to withstand 1,008 passes before failure by permanent deformation and 2,056 passes before failure by mat breakage.
- The filleted design was able to sustain more than twice the number of passes sustained by the non-filleted design before failure by both permanent deformation and mat breakage.

6.2 Recommendations

Based on the airfield mat evaluation described herein, the following recommendations are provided:

- Additional investigation should be conducted to verify the feasibility of increasing the radius of the filleted corner and whether it can provide additional improvement in fatigue life of the end connector rails.

- Damage in the filleted end connector design was noted to shift from the critical stress location to the upper overlap rail. Joint optimization analyses should be conducted to improve this area of the end connector and further increase the fatigue life of the joint.

References

ASTM International. 2007. *Standard test method for CBR of laboratory compacted soils*. Designation: D 1883. West Conshohocken, PA: ASTM International.

_____.2007. *Standard test method for density and unit weight of soil in place by the sand cone method*. Designation: D 1556. West Conshohocken, PA: ASTM International.

_____. 2007. *Standard test methods for liquid limit, plastic limit, and plasticity index of soils*. Designation: D 4318. West Conshohocken, PA: ASTM International.

_____. 2007. *Standard test method for particle size analysis of soils*. Designation: D 422. West Conshohocken, PA: ASTM International.

_____. 2009. *Standard test method for use of the dynamic cone penetrometer in shallow pavement applications*. Designation: D 6951. West Conshohocken, PA: ASTM International.

_____. 2010. *Standard test method for density of soil in place by the drive cylinder*. Designation: D 2937. West Conshohocken, PA: ASTM International.

_____. 2010. *Standard test method for in-place density and water content of soil and soil-aggregate by nuclear methods (shallow depth)*. Designation: D 6938. West Conshohocken, PA: ASTM International.

_____. 2010. *Standard test methods for laboratory determination of water (moisture) content of soil and rock by mass*. Designation: D 2216. West Conshohocken, PA: ASTM International.

_____. 2011. *Standard practice for classification of soils for engineering purposes (USCS)*. Designation: D 2487. West Conshohocken, PA: ASTM International.

_____. 2012. *Standard test method for laboratory compaction characteristics of soil using modified effort*. Designation: D 1557. West Conshohocken, PA: ASTM International.

Garcia, L., T. W. Rushing, and Q. S. Mason. 2012. *Evaluation of Webcore prototype AMX mat system*. ERDC/GSL TR-12-14. Vicksburg, MS: U.S. Army Engineer Research and Development Center.

Garcia, L. T., and T. W. Rushing. 2013. *AM2 sand subgrade sensitivity test*. ERDC/GSL TR-13-10. Vicksburg, MS: U.S. Army Engineer Research and Development Center.

Garcia, L., T. W. Rushing, and Q. S. Mason. 2014a. *AM2 25 CBR subgrade sensitivity test*. ERDC TR-14-7. Vicksburg, MS: U.S. Army Engineer Research and Development Center.

Garcia. L. , T. W. Rushing, B. A. Williams, and C. A. Rutland.2014b. *AM2 100 CBR subgrade sensitivity test*. ERDC TR-14-37. Vicksburg, MS: U.S. Army Engineer Research and Development Center.

Naval Air Warfare Center. 2006. *Expeditionary airfield AM2 mat certification requirements*. NAWCADLKE-MISC-48J200-0011. Lakehurst, NJ: Naval Air Warfare Center, Aircraft Division.

Rushing, T. W., and J. S. Tingle. 2007. *AM2 and M19 airfield mat evaluation for the Rapid Parking Ramp Expansion Program*. ERDC/GSL TR-07-5. Vicksburg, MS: U.S. Army Engineer Research and Development Center.

Rushing, T. W., and N. Torres. 2007. *Prototype mat system evaluation*. ERDC/GSL TR-07-29. Vicksburg, MS: U.S. Army Engineer Research and Development Center.

Rushing, T. W., and Q. S. Mason. 2008. *AM2 15 CBR subgrade sensitivity test for the Rapid Parking Ramp Expansion Program*. ERDC/GSL TR-08-25. Vicksburg, MS: U.S. Army Engineer Research and Development Center.

Rushing, T. W., N. Torres, and Q. Mason. 2008. *AM2 10 CBR subgrade sensitivity test for the Rapid Parking Ramp Expansion Program*. ERDC/GSL TR-08-13. Vicksburg, MS: U.S. Army Engineer Research and Development Center.

Rushing, T. W., L. Garcia, and Q. S. Mason. 2011. *Large-scale 6-CBR prototype mat system evaluation for the AMX Program*. ERDC/GSL TR-11-37. Vicksburg, MS: U.S. Army Engineer Research and Development Center.

Rushing, T. W., L. Garcia, and Q. S. Mason. 2012. *Evaluation of Faun aluminum mat systems*. ERDC/GSL TR-12-32, Vicksburg, MS: U.S. Army Engineer Research and Development Center.

U.S. Army Engineer Research and Development Center. 1995. *Standard test method for determining the California Bearing Ratio of soils*. Designation: CRD-C654-95. Vicksburg, MS: U.S. Army Engineer Research and Development Center.

REPORT DOCUMENTATION PAGE

Form Approved
OMB No. 0704-0188

1. REPORT DATE *(DD-MM-YYYY)*	2. REPORT TYPE	3. DATES COVERED *(From - To)*
August 2015	Final report	

4. TITLE AND SUBTITLE

AM2 Mat End Connector Modeling and Performance Validation

5a. CONTRACT NUMBER

5b. GRANT NUMBER

5c. PROGRAM ELEMENT NUMBER

6. AUTHOR(S)

Lyan Garcia, Timothy W. Rushing, Quint Mason, Jeb S. Tingle, and Craig A. Rutland

5d. PROJECT NUMBER

5e. TASK NUMBER

5f. WORK UNIT NUMBER

7. PERFORMING ORGANIZATION NAME(S) AND ADDRESS(ES)

U.S. Army Engineer Research and Development Center
Geotechnical and Structures Laboratory
3909 Halls Ferry Road
Vicksburg, MS 39180-6199

8. PERFORMING ORGANIZATION REPORT NUMBER

ERDC/GSL TR-15-28

9. SPONSORING / MONITORING AGENCY NAME(S) AND ADDRESS(ES)

Headquarters, Air Force Civil Engineer Center
Tyndall Air Force Base, FL 32403-5319
Under Airfield Damage Repair Modernization Program

10. SPONSOR/MONITOR'S ACRONYM(S)

11. SPONSOR/MONITOR'S REPORT NUMBER(S)

12. DISTRIBUTION / AVAILABILITY STATEMENT

Approved for public release; distribution is unlimited.

13. SUPPLEMENTARY NOTES

14. ABSTRACT

The U.S. Army Engineer Research and Development Center executed a test program for the Air Force Civil Engineer Center and the Naval Air Systems Command that involved a series of full-scale tests of the AM2 airfield mat system in an effort to validate a model that can predict the performance of AM2 under different operational conditions. After completion of the program, a thorough investigation of both the subgrade and the mat revealed that the manufacturer's drawing of the extrusion dye for the AM2 end connector omitted fillets in the corners of the locking bar channel. The efforts of the test program discussed in this report focused on evaluating AM2 with the two different end connector designs (i.e., filleted and non-filleted locking bar slot) and evaluating the performance of each in terms of number of passes to failure. Two sections were tested individually under simulated F-15E aircraft traffic. Mat breakage and permanent deformation were monitored. The AM2 end connector design with the filleted corners was able to sustain more than twice the traffic sustained by the non-filleted design before failure by both permanent deformation and mat breakage.

15. SUBJECT TERMS

AM2, Landing mat, Aluminum mat
Airfield mat
Airfield damage repair
Expeditionary airfield
Airfield mat modeling

16. SECURITY CLASSIFICATION OF:			17. LIMITATION OF ABSTRACT	18. NUMBER OF PAGES	19a. NAME OF RESPONSIBLE PERSON
a. REPORT	b. ABSTRACT	c. THIS PAGE			19b. TELEPHONE NUMBER *(include area code)*
UNCLASSIFIED	UNCLASSIFIED	UNCLASSIFIED		61	